



Lehrstuhl für
Solartechnik

RWTHAACHEN
UNIVERSITY

The present work was submitted to the
DLR - Institute of Solar Research, Chair of Solar Technology

Reducing the Impact of Irradiance Ramps on PV Power Production – A Techno-Economic Analysis of Nowcasting

Master Thesis

presented by
Höpken, Lars
420837

Univ.-Prof. Dr.-Ing. Robert Pitz-Paal
M.Eng. Tim Kotzab
Dr.-Ing. Bijan Nouri

Aachen, 28.07.2023

Reducing the Impact of Irradiance Ramps on PV Power Production – A Techno-Economic Analysis of Nowcasting

Lars Höpken

Abstract

Electricity grids experience an increasing amount of volatile renewable energy integration. This introduces new challenges for the stable operation of the grid and the matching of supply and demand. One of the technical challenges relates to unforeseen short-term power ramps being transmitted to the electrical grids. Such ramps in power production can disrupt grid stability, leading to imbalances, fluctuations in frequency and voltage, potential equipment failures and power outages. Furthermore, they can affect electricity market dynamics, causing price fluctuations. For photovoltaic (PV) power plants the primary source of short-term variability are irradiance ramps caused by clouds.

All-sky imagers offer the potential to analyse the current sky conditions and produce shortest-term forecasts (nowcasts) of the irradiance up to 20 minutes into the future. This work investigates the potential of nowcasts for mitigating power ramps through preventive curtailment and analyses the associated economic consequences. For this purpose, irradiance nowcasts for a time frame of one year are fed into a virtual PV plant model located in southern Spain. The model simulates the power output of the plant and thereby processes the irradiance nowcasts into power nowcasts. Several ramp mitigation strategies based on the power nowcasts are developed and assessed. These nowcasting strategies are benchmarked against battery storage strategies, as well as hybrid strategies combining nowcasting and battery storage. The economic performance of the configurations is analysed and compared. For this, an incentive for power smoothing in the form of a monetary penalty for missed ramps is introduced. A simplified simulation of the marketing of the produced electricity determines yearly profits for every configuration which are then used in combination with the overall system costs to calculate the net present values.

Using the net present value as a benchmark, a hybrid configuration is found to be the optimal solution for the power control under the applied regulatory framework. It is able to reduce the number of ramps by 93 % while reducing the required battery size by 40 % in comparison to a standalone storage solution. However, the analysis also shows that the introduction of ramp rate regulation and the consequent investment in ramp mitigation and curtailment of energy leads to overall higher levelized costs of energy and lower net present values.

Contents

Figures	VI
Tables	VII
Abbreviations	VIII
1. Introduction.....	1
2. State of the art.....	2
2.1. Solar irradiance.....	2
2.2. Photovoltaics.....	3
2.3. Electricity markets	4
2.4. Regulations	6
2.5. Nowcasting.....	7
2.6. Energy storage.....	9
2.7. Simulation design.....	10
3. Use cases	12
3.1. Components	12
3.1.1. PV system	12
3.1.2. Storage.....	16
3.1.3. Nowcasting system	19
3.2. Configurations.....	19
3.3. Regulations	20
3.3.1. Ramp rate limit.....	20
3.3.2. Penalties	21
4. Methodology.....	24
4.1. Preprocessing	25
4.2. Simulation	27
4.3. Postprocessing.....	28
4.3.1. Power control strategies	29
4.3.2. Marketing strategy.....	36
4.3.3. Economic analysis.....	38

5. Results	40
5.1. Simulation results.....	40
5.2. Power control algorithms	43
5.2.1. Single day performance analysis	43
5.2.2. Full year performance analysis	47
5.3. Economic results	49
5.3.1. Base case and ideal nowcast	49
5.3.2. Penalties	50
5.3.3. Nowcast and storage	53
5.3.4. Optimization and hybrid.....	55
5.4. Sensitivity analysis.....	62
6. Conclusion.....	66
7. Bibliography	69
Appendices	76
A. PV module parameters.....	76
B. Factors for nowcast weighting	76
C. Detailed inputs and results	77

Figures

Figure 2.1: Relevant irradiance metrics for PV power generation	2
Figure 2.2: Cumulative power capacity by technology	3
Figure 2.3: Illustration of processing steps for the generation of nowcast irradiance maps	7
Figure 2.4: Illustration of the hybrid nowcasting model	8
Figure 2.5: Basic structure of the simulation tool	11
Figure 3.1: Plot of the simulated PV plant at CIEMAT's PSA	13
Figure 3.2: Ramp rate calculation methods	20
Figure 3.3: Visualization of ramp rate violation energy calculation	22
Figure 4.1: Workflow schematic of the calculations and processes carried out	24
Figure 4.2: Example of a DNI validation map generated from measurements at the meteo stations	26
Figure 4.3: Power control with selection of strategies and associated inputs and outputs	29
Figure 4.4: Flowchart of the base case power control strategy	30
Figure 4.5: Flowchart of the storage power control strategy	30
Figure 4.6: Flowchart of the nowcast power control strategy	32
Figure 4.7: Exemplary interim results of the nowcast smoothing process	34
Figure 4.8: Flowchart of the hybrid power control strategy	35
Figure 4.9: Marketing strategy with the sub-modules day-ahead, imbalance, storage and penalties	36
Figure 5.1: Validation irradiance and power curves for an exemplary day	40
Figure 5.2: Box plots of AC power error metrics	42
Figure 5.3: Performance charts of base case and ideal nowcast for one exemplary day	44
Figure 5.4: Performance charts of storage and nowcasting configurations for one exemplary day	45
Figure 5.5: Performance charts of hybrid configurations for one exemplary day	47
Figure 5.6: Economic comparison of nowcasting and designed storage configurations	54
Figure 5.7: Sensitivity analysis of the net present value to different maximum storage powers	56
Figure 5.8: Economic comparison of optimized storage and hybrid configurations	61
Figure 5.9: Sensitivity analysis of the net present value to seven different parameters	63

Tables

Table 2.1: Overview of regulations in different grid codes.....	6
Table 2.2: Description of DNI variability classes.....	9
Table 3.1: Characteristics of the PV power plant.....	15
Table 3.2: Battery CAPEX for different storage durations and powers in 2023	18
Table 3.3: Characteristics of the storage system.....	18
Table 3.4: Characteristics of the nowcasting system.....	19
Table 5.1: Bias, RMSE and MAE of the AC power of the complete year	41
Table 5.2: Performance comparison of all major strategies for the complete year ...	48
Table 5.3: Economic comparison of base case and ideal nowcast	50
Table 5.4: Necessary values for penalty factor calculation	51
Table 5.5: Comparison between fee and tax penalty schemes	53
Table 5.6: Optimized maximum storage powers.....	57
Table 5.7: Detailed inputs of the hybrid weighted configuration	58
Table 5.8: Detailed results of the hybrid weighted configuration	59
Table 5.9: Performance comparison of strategies with optimized storages for the complete year	60
Table 6.1: Overview of selected final results	67
Table A.1: PV module parameters	76
Table B.1: Factors for nowcast weighting.....	76
Table C.1: Detailed inputs of all presented configurations	77
Table C.2: Detailed results of all presented configurations.....	79

Abbreviations

AC	Alternating current	GTI	Global tilted irradiance
ASI	All-sky imager	IRENA	International Renewable Energy Agency
BESS	Battery energy storage system	LCOE	Levelized cost of energy
BRP	Balancing responsible party	LIB	Lithium-ion battery
BSP	Balancing service provider	LT	Lead time
CAPEX	Capital expenditure	LTO	Lithium-titanium-oxide
CEC	California Energy Commission	MAE	Mean average error
CIEMAT	Centro de Investigaciones Energéticas, Medioambientales y Tecnológicas	NPV	Net present value
CO ₂	Carbon dioxide	NREL	National Renewable Energy Laboratory
CRPS	Continuous ranked probability score	NWP	Numerical weather predictions
DC	Direct current	OPEX	Operational expenditure
DHI	Diffuse horizontal irradiance	PSA	Plataforma Solar de Almería
DLR	German Aerospace Center	PV	Photovoltaics
DNI	Direct normal irradiance	RMSE	Root mean square error
ETR	Extraterrestrial radiation	SOC	State of charge
EU	European Union	TSO	Transmission system operator
GHI	Global horizontal irradiance	VRE	Variable renewable energy
		WACC	Weighted average cost of capital
		YACOP	Yield Assessment Computation and Optimization Program

1. Introduction

Climate change is the primary driver of the current and future transformation of the world's energy systems. The unsustainable, large scale burning of fossil fuels for electricity generation is gradually being replaced by renewable energy sources in order to reduce CO₂ emissions. The European Union (EU) and many national governments have adopted policies to increase the amount of renewable energy production significantly. In March of 2023 the EU agreed on stronger legislation to accelerate the rollout of renewable energy [1]. This agreement included a raise of the binding renewable target for 2030 from 32 % to 42.5 % and formulated the aim to reach 45 %.

A major challenge for energy system operators is the volatility related to the increasing integration of renewables [2-6]. In the case of solar power generation, the fluctuations are mainly caused by changes in solar irradiance (e.g. by passing clouds). As discussed in [4], rising integration of these variable renewable energy (VRE) sources results in an increase in net load ramp magnitudes and ramp frequency and thus will lead to a growing requirement of highly flexible power plants, demand-side response and energy storage.

Some grid operators have already imposed restrictions on the variability of the power output of VRE plants [7-9]. Most commonly the ramp rate of the output is limited to 10 % of the rated power per minute. The conventional approach to adhere to these restrictions is to use large battery energy storage systems (BESS) and smooth the power output this way. However, this adds significant capital costs [10, 11]. Many studies therefore propose the implementation of shortest-term forecasts or nowcasts in order to predict ramp events and reduce the required storage capacity [11-14].

This thesis is investigating the potential of all-sky imager (ASI) based nowcasts to reduce the impact of irradiance ramps on a virtual photovoltaic (PV) system in southern Spain. Real irradiance data and nowcasts for a timeframe of one year are used to simulate the output of the PV system. A techno-economic analysis aims to compare different nowcast and storage configurations while implementing a penalty scheme for missed ramps. An overview of the state of the art is given in chapter 2. Chapter 3 defines the use cases while the methodology is explained in chapter 4. Finally, the results of the simulation and analysis are presented in chapter 5.

2. State of the art

This chapter will provide the groundwork of the topics relevant for this thesis. First the basics of solar and more precisely photovoltaic power production are presented. Then, an overview of energy markets and the process of trading electricity is given. Next, current regulations in different grid codes are summarized, followed by the state of the art in nowcasting and energy storage technology. Finally, the design of the simulation tool used is described.

2.1. Solar irradiance

When analysing a solar power plant, it is important to define the relevant irradiance measures that directly influence the power generation. Figure 2.1 depicts the three most important ones. The direct normal irradiance (DNI) refers to the irradiance coming from the sun disk itself, measured on a surface perpendicular to the beam. Scattered radiation from the sky dome (excluding the sun disk) is called diffuse horizontal irradiance (DHI). Together with the direct irradiance it makes up the global horizontal irradiance (GHI). Both are relative to a horizontal surface. The global tilted irradiance (GTI) refers to the irradiance a tilted surface (e.g. a solar panel) actually receives. It includes direct and diffuse irradiance, as well as reflected irradiance from the ground [15].

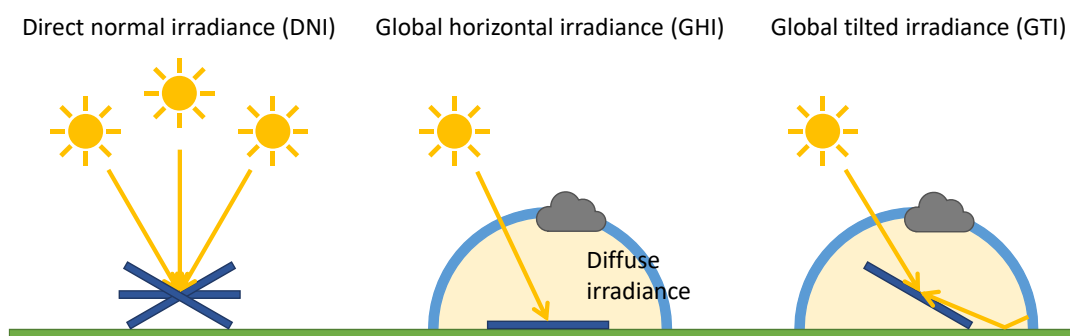


Figure 2.1: Relevant irradiance metrics for PV power generation [16]

The DNI that reaches the ground is not equal to the extraterrestrial radiation (ETR) provided by the sun. The atmosphere acts as a filter, scattering and reducing the intensity of the irradiance. The path length the photons have to travel through the

atmosphere varies with the sun's position, more precisely with the solar zenith angle. This behaviour is modelled by the air mass value. It is set to equal 1 at solar noon and increases proportionally to the path length with lower inclinations [15].

2.2. Photovoltaics

Solar PV is the most rapidly growing technology in electricity generation [17]. Figure 2.2 shows the historic and forecasted development of the cumulative power capacities for each technology. Solar PV overtook wind power in 2020 and is set to even surpass coal by 2027.

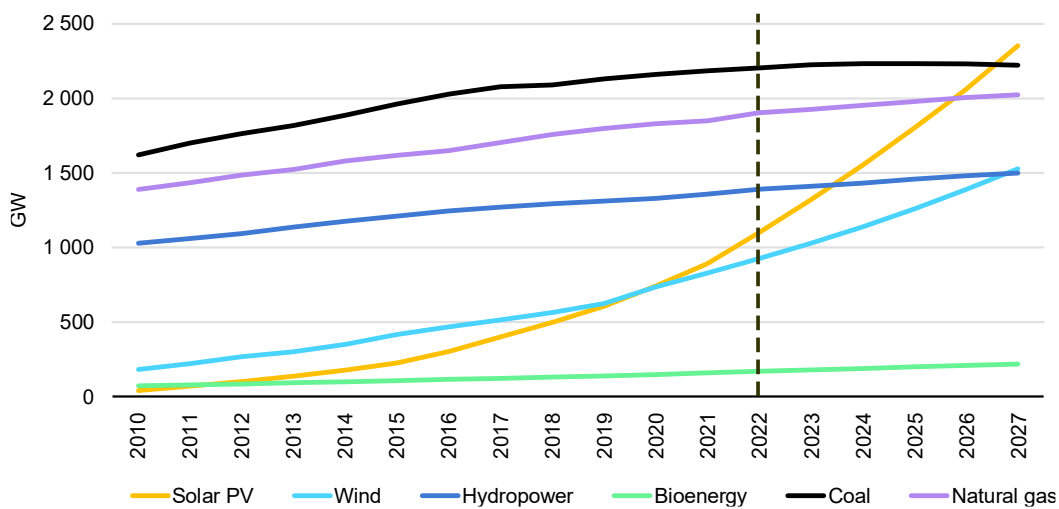


Figure 2.2: Cumulative power capacity by technology, historic data from 2010 – 2022 and projection until 2027. Taken from [17]

This section provides a brief overview of the operating principle of PV cells and the structure of typical PV power plants.

The underlying principle of power generation with a PV cell is the photoelectric effect, first described by Albert Einstein in 1905 [18]. It occurs when photons interact with electrons in the valence band of a semiconductor, transfer their energy and excite the electrons to the conduction band.

In order to take advantage of this effect, PV cells consist of a pn-junction, a combination of two semiconductors, one p-type and one n-type. The two types of semiconductors are doped with atoms of a higher or lower main group than the base element (typically Silicon). This results in free electron holes in the p-type semiconductor and free electrons in the n-type semiconductor. When brought together to a pn-junction, the free charge carriers diffuse into the opposite material,

creating a space charge region and an electric field. When the cell is exposed to irradiation and electrons in the p-type region are excited to the conduction band, they are influenced by the electric field and move to the n-type region, leaving holes in the p-type region. Depending on whether the contacts are open or shorted, either a voltage (open-circuit voltage) or a current (short-circuit current) can be observed. When connected to a load instead, a power output is generated [19]. Current state-of-the-art multicrystalline Silicon cells have an efficiency of up to 23.3 % [20].

To create a PV module, several cells are connected and encased in a protective housing. Multiple modules put together form a PV array. Since the output of each cell and thus of the whole array is direct current (DC) power, inverters are used for transformation to an alternating current (AC) output. The inverters also are responsible for the maximum power point tracking, setting their impedance in such a way that the voltage and current in the cells result in the maximum power output. Different strategies exist concerning the amount and connection of the inverters. One central inverter may save investment costs, however smaller single-string or multi-string inverters lead to higher availability and higher efficiencies since each sub-array can be optimized for maximum power output [21].

2.3. Electricity markets

All generators, e.g. PV power plants, participate in certain markets in order to sell their produced electricity. These electricity markets ensure that the ratio between consumption (energy bought from the markets) and production (energy sold to the markets) is always kept in balance and the grid remains in a stable operating point.

While there is no standard for the implementation of electricity markets, most zones operate under similar principles and divide the trading into the same following submarkets [22].

Day-ahead market

As the name suggests, trading on the day-ahead market takes place on the day before delivery, usually until 12 o'clock. The electricity price is determined by bidding of sellers and buyers. The sellers (generators) as well as the buyers (consumers) place offers and bids consisting of a price and a quantity. The market operator sorts them by price, in an increasing order for the offers by the sellers and a decreasing order for the bids by the buyers. The point where the resulting supply and demand curves intersect determines the final price. This price is then applied to all generators. Depending on the exact pricing scheme, locational and grid information may also be considered [22, 23].

This way an electricity price for every hour of the following day is determined and energy traded accordingly. The prices are publicly available at the ENTSO-E Transparency Platform [24].

Intraday market

Because of the time delay between day-ahead market closure and delivery, new information about the actual demand and supply may arise within this time frame. A high penetration of renewables especially amplifies the deviations from the day-ahead forecast. To deal with these discrepancies, electricity is traded on the intraday market until shortly before physical delivery. Two trading procedures exist, an auction-based one, similar to the day-ahead market, and the nowadays more widespread continuous trading. The continuous market offers an uninterrupted service and bids made to the platform are matched automatically. The resolution of traded positions can vary from 60 to 15 minutes and trading may be possible until just five minutes before delivery [22, 23].

The Iberian market, which Spain is participating in, uses both, an auction-based and a continuous intraday market. The auction market consists of six trading sessions per day and allows trading until four hours before delivery. Trading until two hours before delivery is possible in the continuous market [25, 26].

Intraday prices are usually published by the market operators [27].

Balancing market

The last instance for maintaining equality between production and consumption is the balancing market. It is operated by the responsible transmission system operator (TSO) to ensure grid stability and maintain the nominal frequency. Some market entities may need to update their generation or consumption close to real time, causing an imbalance in the grid. These entities are called balancing responsible parties (BRPs) and are financially liable for their imbalances. The price is determined by trading between so called balancing service providers (BSPs) and the TSO who has to procure the corresponding balancing services caused by the responsible parties [22].

The Spanish TSO implements a dual imbalance pricing scheme, charging or remunerating the BRP depending on whether the imbalance goes in the same direction as the system imbalance or in the opposite direction, thus helping to restore the balance. Additionally, different prices are applied depending on the sign of the imbalance. This is due to the costs of balancing regulation being different for up- and downward regulation [28]. While “helping” imbalance is remunerated with the day-ahead market price, “amplifying” imbalance is charged with either the up- or downward imbalance price. In Spain these prices are published by the TSO “Red Eléctrica” [29].

2.4. Regulations

In addition to the markets, every electricity grid has a technical regulatory framework which all participating parties have to comply with. These regulations encompass for example frequency and voltage control, reactive power provision, fault behaviour, general connection requirements and active power control [30]. Especially the last item is relevant for this thesis since it may include the limitation of gradients in the power output.

Table 2.1: Overview of regulations in different grid codes

Country	Active power management	Ramp rate limit	Penalties
Australia	Required, except VRE [31, 32]	Western Power: $\pm \max(10 \text{ MW}/\text{min}, 15 \text{ \%/min})$ except VRE [33]; Horizon: $\pm 15 \text{ \%/min}$ including VRE [34] (low voltage: [35])	“causer pays” for frequency control, factors recalculated every four weeks based on historical data [36, 37]
China	Required, including forecasts [38]	$\pm 10 \text{ \%/min}$ [38]	–
Denmark	Required [39]	$\pm 100 \text{ kW/s}$ [39]	–
Ethiopia	Required [40]	-10 \%/min [40]	–
Germany	Required [41, 42]	$0.33 \text{ \%/s} < r < 0.66 \text{ \%/s}$ (after receiving instruction) [41]	–
Hawaii	–	$\pm 2 \text{ MW}/\text{min}, \pm 1 \text{ MW/s}$ [7]	–
India	Required [43]	$\pm 10 \text{ \%/min}$ [43]	–
Ireland	Required [44]	$+30 \text{ MW}/\text{min}$ [7]	–
Malaysia	Required [45]	$\pm 15 \text{ \%/min}$ [46]	–
Puerto Rico	Required [7, 47]	$\pm 10 \text{ \%/min}$ [7, 47]	Curtailement depending on compliance rate on a weekly basis [48]
Spain	Required [49, 50]	–	–

Many countries require some form of active power management in order to react to dispatch instructions and control their power output according to instructions by a control centre. Additionally, their grid codes often contain limitations for up or down gradients in the power output. However, some of these grid codes make the compliance requirement depending on energy source availability, thus excluding VRE

sources from those regulations. Even fewer codes implement penalties for non-compliance with the rules. Often just stating compliance as required for connection. Table 2.1 shows some of the regulations currently implemented worldwide.

Further regulations applying to PV systems are listed in [8]. They are however not considered in this analysis.

2.5. Nowcasting

Numerical weather predictions (NWP) can generate forecasts up to several days ahead with temporal and spatial resolutions of 1 h and 1 km respectively. Satellite-based forecasting solutions achieve a higher temporal resolution of 15 min with a horizon of 6 h and spatial resolution of 2 km [51]. However, both of these systems fall short when it comes to intra-hour up to intra-minute forecasts with high temporal and spatial resolutions. Since the availability of the solar resource is highly volatile and dependent on cloud movement, shortest-term forecasts or nowcasts are introduced to fill this gap. One common approach for generating nowcasts involves the utilization of all-sky imagers (ASIs), which are 180° fish-eye cameras directed towards the sky [14]. The system used in this thesis was developed at the German Aerospace Center (DLR) and utilizes the images from two cameras to create nowcasts with a spatial resolution of 20 metres, a temporal resolution of 30 seconds and a forecasting horizon of up to 20 minutes [51]. These nowcasts come in the form of DNI and GHI irradiance maps of the area around the camera setup.

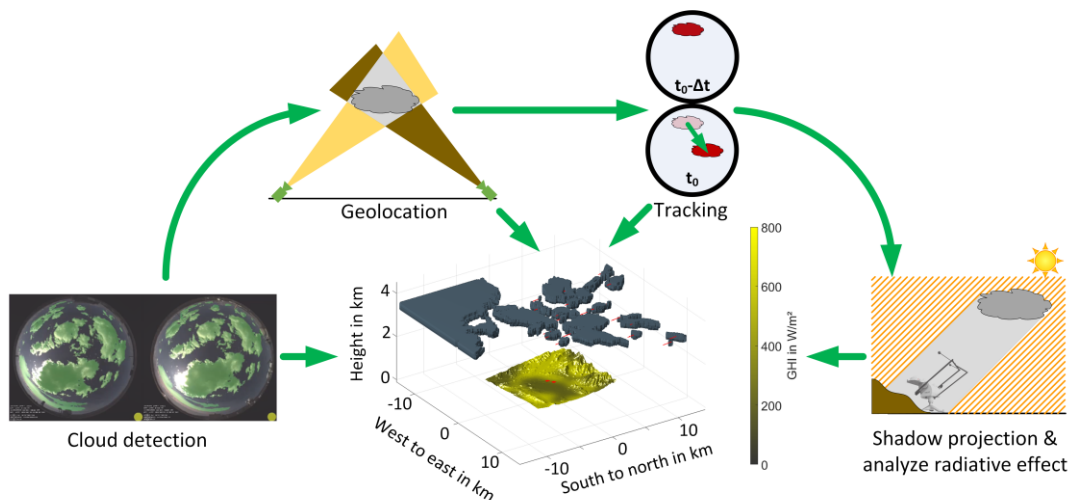


Figure 2.3: Illustration of processing steps for the generation of nowcast irradiance maps. Taken from [51]

Several steps are necessary to process the all-sky images and generate a nowcast. The underlying process is shown in Figure 2.3. First, the images are analysed and potential clouds are detected. Using a stereoscopic approach, the clouds are geolocated and then tracked over time. Finally, the radiative effect is analysed and the shadow projected to the ground, resulting in an irradiance map. These maps are generated for the current and every predicted cloud formation [51]. Besides the camera images, measurements of the present DNI and DHI are also incorporated.

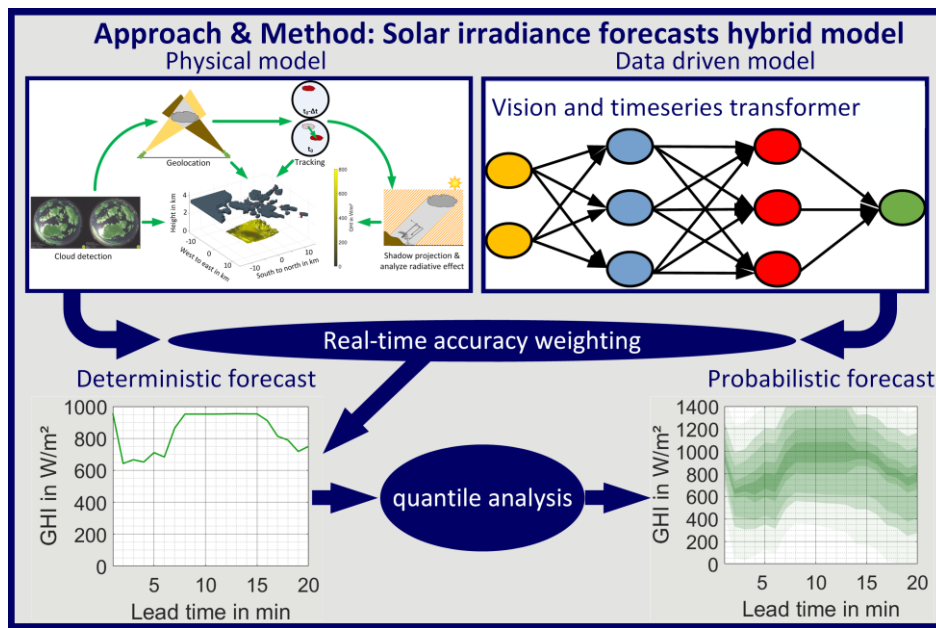


Figure 2.4: Illustration of the hybrid nowcasting model

In its current implementation (illustrated in Figure 2.4) the nowcasting system has been enhanced with an additional data driven machine learning model [52]. Recent outputs of the previously described physical model and the data driven model, are benchmarked against each other in real time. This results in dynamic accuracy weights, which are used to combine both approaches into a single deterministic nowcast. The combined forecast benefits from the strengths of the models in different conditions. The bottom left graph in Figure 2.4 shows how the GHI forecast for one grid point of the area under study might look like. Since the deterministic forecasts are subject to significant uncertainties, reliable information about these uncertainties is necessary in order to enable the practical utilization of nowcasts. Consequently, it is crucial for these nowcasts to adopt a framework that offers probability distributions. In this work, probabilistic nowcasts are obtained by the outcomes of a quantile analysis applied to the deterministic nowcasts [53]. First, the present irradiance condition receives a classification according to Table 2.2, based on recent historical ground

measurements. Looking at historical nowcast errors for equally classified conditions, different percentiles are calculated, which make up the outlines of the prediction intervals shown in the bottom right graph of Figure 2.4. The deterministic forecast would be in the middle of the darkest region and equal the percentile P50, meaning that 50 % of the time the actual value is expected below this line. Following the same logic, the pair of the percentiles P20 and P80 for example spans the area where the actual irradiance is below or above 20 % of the time respectively, resulting in the 60 % prediction interval. Lighter shading therefore means higher prediction intervals. Depending on the variability of the conditions and consequent classification, the intervals have a higher or lower spread [53]. The final output of the nowcasting system is a set of probabilistic DNI and GHI maps for each percentile with a 1-minute resolution and up to 20 minutes into the future. These forecasting times are referred to as lead times (LT). Each nowcast therefore contains irradiance maps for LT0 (current conditions) up to LT20 [53]. A new nowcast is generated every 30 seconds.

Table 2.2: Description of DNI variability classes. Based on [54]

Class	Sky conditions	Variability
1	Mostly clear sky	Low variability
2	Almost clear sky	Low variability
3	Almost clear sky	Intermediate variability
4	Partly cloudy	High variability
5	Partly cloudy	Intermediate variability
6	Partly cloudy	High variability
7	Almost overcast	Intermediate variability
8	Mostly overcast	Low variability

2.6. Energy storage

Due to the increase in VRE implementation, the demand for energy storage has never been higher. Many different kinds of energy storage technologies exist [55]. Each with its own ideal use case. PV power plants are most often combined with electro-chemical storage systems, namely BESS. They are used to provide a multitude of different services such as frequency regulation, energy shifting, curtailment reduction and ramp rate control [56, 57]. Lithium-ion batteries (LIB) are by far the most common technology for large scale installations [56, 58].

An important metric for storage systems is the ratio between energy capacity and maximum power, often referred to as C-rate. A C-rate of 1 implies that a battery's energy and power rating have the same value and thus a discharge at full power would last for one hour. This is referred to as a 1-h storage [59].

Typical utility scale batteries possess a C-rate of around 1 with some exceptions reaching C-rates of up to 2 [56, 58]. However, even though not currently implemented in utility scale applications, high-power LIB cells, more precisely Lithium-titanium-oxide (LTO) batteries do exist and are capable of much higher C-rates [55, 59]. The maturity level of this technology is assessed to be in “early commercialisation” by the International Renewable Energy Agency (IRENA) [59]. In their “Study on Energy Storage” [60] the EU Commission attests these high-power LIBs their suitability for ancillary services such as ramp rate control.

2.7. Simulation design

A central part of this thesis is the simulation tool that emulates the PV system under study and calculates a power output for every time step of the irradiance inputs. This tool has been developed in a previous master thesis by Jonas Schaible and the reader is referred to this reference for a detailed description of the simulation design and the inner workings [16]. This section only provides a rough overview of the general structure and main processes.

The foundation of the tool is the Yield Assessment Computation and Optimization Program (YACOP) developed at DLR [61]. It is written in Python and was designed for yield prediction of concentrated solar power plants. In order to achieve flexibility regarding the inputs and modes of operation, it is structured in a modular fashion. The main inputs are time series which are processed by the time series calculator. Each time step of a series is passed to a time step solver which distributes the inputs and parameters to the system level, containing the system under study and carrying out the calculations. In this case, a detailed PV model based on the “pvlib python” package [62] has been implemented as the system level, containing several sub-systems. Figure 2.5 shows the basic structure of the system level with the sub-systems “Irradiance Analysis”, “PV Array” and “Inverter”. The procedure starts with the irradiance nowcasts and information about the plant as inputs. First, the irradiance analysis selects the percentile to use for further calculations based on the classification of the current conditions (section 2.5). These selected nowcasts are passed to “PV Array” and then “Inverter” where first the DC power for each module and then the AC power per inverter is calculated. This is repeated for all available lead times at every time step, resulting in a nowcast of the PV plant power.

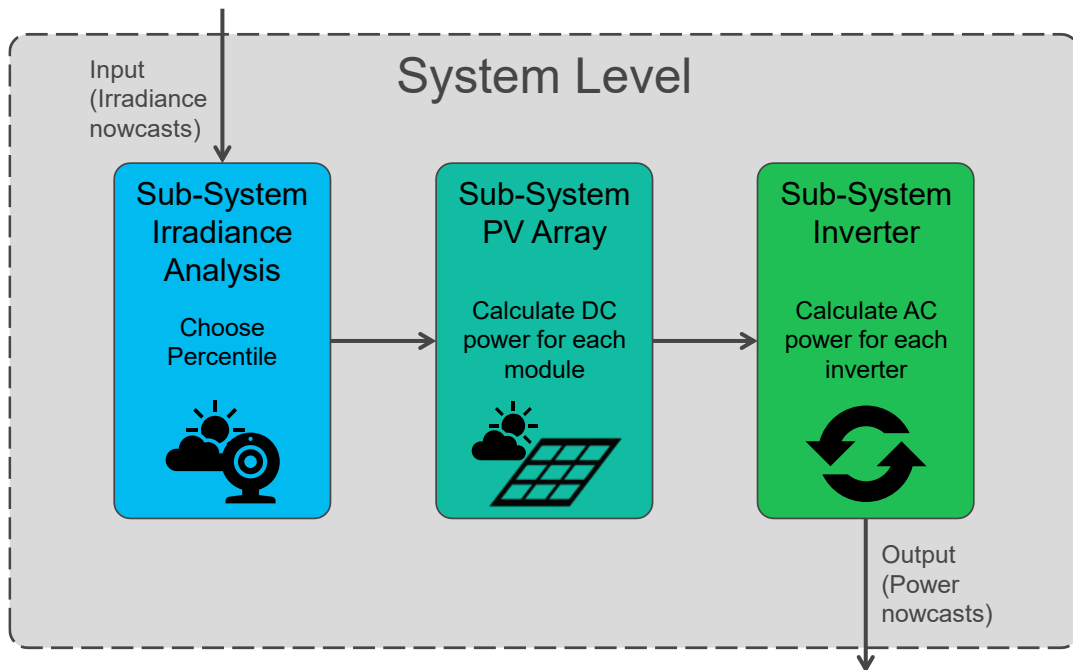


Figure 2.5: Basic structure of the simulation tool

Further details regarding the calculations and adaptations in the current implementation are presented in section 4.2.

3. Use cases

This chapter introduces the use cases that are investigated in this thesis. A use case always represents a combination of a configuration and a set of regulations. The configuration defines the details of the setup under study, while regulations specify the restrictions imposed by the grid code. In order to create viable configurations, the components used need precise definition.

3.1. Components

The relevant components for this thesis are the PV system, the storage system and the nowcasting system. All three of them are designed and parameterised in the following sections.

3.1.1. PV system

The central component of each configuration is the PV system itself. A virtual power plant is placed in the location of the Plataforma Solar de Almería (PSA) operated by the Centro de Investigaciones Energéticas, Medioambientales y Tecnológicas (CIEMAT). The site was chosen based on the availability of nowcasts and meteorological reference signals.

Measurements taken from satellite images of existing plants are taken as a baseline for getting typical dimensions and orientations. Additionally, a PV module is selected from the California Energy Commission's (CEC) module database [63] and missing parameters are extracted from the Sandia National Laboratories module database [64]. Appendix A contains a complete list of the parameters used.

A total of 78,400 modules make up the final PV system. These modules are connected into strings which themselves are connected to inverters. Each row of the plant consists of four strings and two inverters. The general setup as well as a detailed depiction of the different strings is shown in Figure 3.1.

Since the simulation makes use of the simplified PVWatts inverter model [65], only two inverter parameters need to be defined. First, the required maximum DC power capability of the inverter $P_{DC,inv}$ is calculated according to Equation (3.1) and rounded up to ensure a safety margin. The values for the DC power of one module $P_{DC,mod}$,

number of modules per string $n_{mod, str}$ and number of strings per inverter $n_{str, inv}$ are listed in Table 3.1.

$$P_{DC, inv} = P_{DC, mod} * n_{mod, str} * n_{str, inv} \quad (3.1)$$

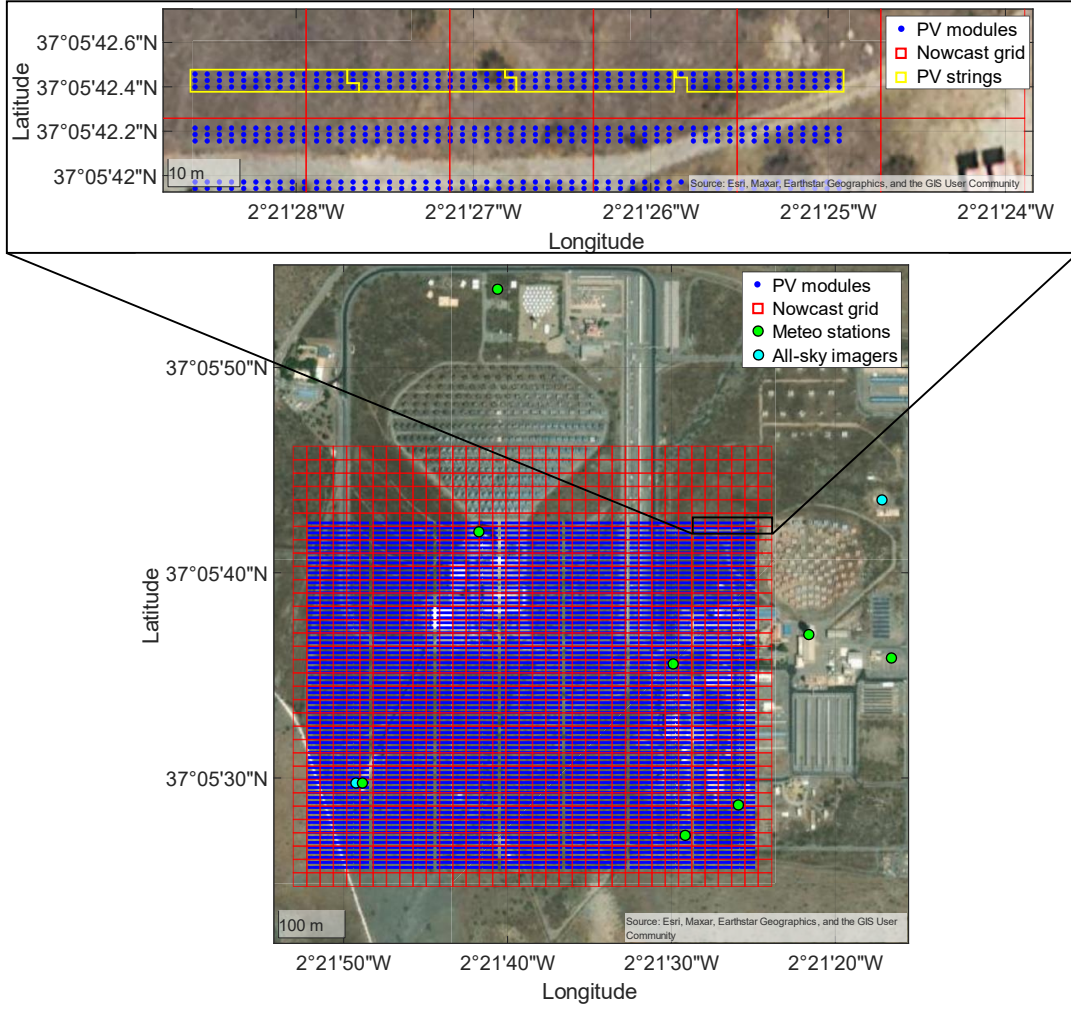


Figure 3.1: Plot of the simulated PV plant at CIEMAT's PSA. Each yellow outline represents one string of PV modules

Second, the nominal efficiency is set to $\eta_{inv, nom} = 0.98$, which corresponds to a modern inverter in this power range [66]. These two values determine the maximum AC power output of one inverter $P_{AC, inv}$ (Eq. (3.2)).

$$P_{AC, inv} = \eta_{inv, nom} * P_{DC, inv} \quad (3.2)$$

The theoretical maximum total power output of the plant $P_{PV,max}$ is calculated by multiplying the AC power of one inverter with the total amount of inverters n_{inv} (Eq. (3.3)) and equals a little over 21 MW.

$$P_{PV,max} = P_{AC,inv} * n_{inv} \quad (3.3)$$

In order to account for losses in the process chain, several correction factors are implemented (section 4.2). The simulation uses the default values, taken from [65].

One central assumption in this thesis is the presence of an active power controller, which is able to precisely adjust the output power according to the current needs. This assumption is reasonable since such a device is required by many grid codes (see section 2.4) and also has been used by other publications [14].

Lastly, the lifetime and costs of the PV system need to be defined for later use in the economic analysis (section 4.3.3). The lifetime is set to 30 years according to [10] and [67]. The investment costs vary significantly depending on the country. While module prices are relatively similar, costs for the remaining hardware, installation and other soft costs like design and financing can be very different [68]. Considering this, the 2021 investment costs for Spain were taken as a baseline for a 2023 estimation using the forecasted cost evolution of the National Renewable Energy Laboratory (NREL) [69]. NREL expects the utility-scale PV cost to sink by roughly 7.9 % from 2021 to 2023. Taking a currency conversion factor of 0.9 into account, Equation (3.4) gives the final PV investment costs used for this analysis (values extracted from [68, 69]).

$$CAPEX_{PV} = 816 \frac{\text{USD}}{\text{kWp}} * (1 - 0.079) * 0.9 \frac{\text{EUR}}{\text{USD}} = 676.38 \frac{\text{EUR}}{\text{kWp}} \quad (3.4)$$

Since operating costs for Spain are not available, costs for Germany are taken instead. Again applying the United States NREL costs forecast, Equation (3.5) yields the final operating costs (values extracted from [67, 69]).

$$OPEX_{PV} = 13.3 \frac{\text{EUR}}{\text{kWp} * \text{a}} * (1 - 0.0585) = 12.52 \frac{\text{EUR}}{\text{kWp} * \text{a}} \quad (3.5)$$

The following Table 3.1 summarizes all relevant characteristics of the PV system.

Table 3.1: Characteristics of the PV power plant

	Parameter	Value
PV module [63]	Name	REC_Solar_REC265PE
	Technology	Multi-crystalline Silicon
	Name plate power ($P_{DC,mod}$)	265.122 W
Inverter	Maximum DC power ($P_{DC,inv}$)	22,000 W
	Nominal efficiency ($\eta_{inv,nom}$) [66]	0.98
	Maximum AC power ($P_{AC,inv}$)	21,560 W
	Modules per string ($n_{mod,str}$)	40
	Strings per inverter ($n_{str,inv}$)	2
	Number of inverters (n_{inv})	980
Correction factors [65]	Soiling factor ($corr_{SF}$)	0.98
	Wiring ($corr_W$)	0.98
	Mismatch ($corr_{MM}$)	0.98
	Light-induced degradation ($corr_{LID}$)	0.985
	Connections ($corr_C$)	0.995
	Nameplate rating ($corr_{NR}$)	0.99
	Availability ($corr_A$)	0.97
Geometry	Modules per row	160
	Modules above each other	3
	Row distance (incl. modules)	7.5 m
	Rows per block	70
	Block distance	5.6 m
	Number of blocks	7
	N-S dimension	519.3 m
	E-W dimension	671.7 m
	Azimuth	180°
Tilt	30°	
Geography	Latitude	37.0927°
	Longitude	-2.3607°
	Altitude	546 m
	Albedo [70]	0.14
PV system	Maximum power ($P_{PV,max}$)	21,128,800 W
	Number of modules	78,400
	Lifetime (L_{PV}) [10, 67]	30 a
	Investment costs ($CAPEX_{PV}$) [68, 69]	676.38 EUR/kWp
	Operating costs ($OPEX_{PV}$) [67, 69]	12.52 EUR/kWp/a

3.1.2. Storage

Some of the analysed configurations incorporate a storage system. While both, storage capacity and power, are variables in the subsequent analysis, a baseline for these values still needs to be defined. The state-of-the-art method for ramp-rate-smoothing storage dimensioning is the worst fluctuation model introduced by [57] and improved by [71]. This model assumes an exponential decay of 90 % of the rated power with a time constant τ , which is dependent on the shortest dimension l of the solar field (see Eq. (3.6)).

$$\tau = 0.042 \frac{\text{s}}{\text{m}} * l - 0.5 \text{ s} = 21.3106 \text{ s} \quad (3.6)$$

Using a ramp rate limit of $r_{lim} = 10 \frac{\%P_{pv,max}}{\text{min}} = 0.1667 \frac{\%P_{pv,max}}{\text{s}}$ and $P_{PV,max} = 21,128.8 \text{ kW}$, the maximum necessary storage energy $E_{bat,max}$ is calculated in Equation (3.7) [57]. To compensate both, down and up ramps, the capacity $C_{bat,max}$ is set to double the necessary energy (Eq. (3.8)).

$$E_{bat,max} \approx \frac{0.9 * P_{PV,max}}{3600} \left[\frac{90}{2 * r_{lim}} - \tau \right] = 1313.63 \text{ kWh} \quad (3.7)$$

$$C_{bat,max} = 2 * E_{bat,max} = 2627.26 \text{ kWh} \quad (3.8)$$

[71] proposes to limit up ramps through curtailment by the inverters instead of using the storage and therefore skips the doubling of the capacity. This however leads to the requirement of keeping the storage at a state of charge (SOC) of 100 % while idling. Since such high SOCs result in a significant increase in calendar ageing [72] and SOCs around 50 % are to be preferred, the doubled capacity is kept for this analysis. The second relevant parameter of the storage system is the maximum power for charging and discharging $P_{bat,max}$. Using the same inputs as before, Equation (3.9) gives the power required for the worst fluctuation [57].

$$\begin{aligned} P_{bat,max} &= \frac{P_{PV,max}}{100} * \left[90 - \tau * r_{lim} \left(1 + \ln \left(\frac{90}{\tau * r_{lim}} \right) \right) \right] \\ &= 15,839.76 \text{ kW} \end{aligned} \quad (3.9)$$

Using Equation (3.10) the C-rate CR is calculated.

$$CR = \frac{P_{bat,max}}{C_{bat,max}} = 6.029 \quad (3.10)$$

As stated in section 2.6, current LIB systems usually possess a C-rate of around 1. Applying this limit to the current configuration either means a storage power reduction by a factor of six, leading to the inability to smooth a significant amount of ramp events, or a respective increase in storage capacity, driving up the total costs. For the baseline the second option has to be chosen and results in a final battery capacity of $C_{bat,1h} = 15,839.76 \text{ kWh}$ (Eq. (3.11)).

$$C_{bat,1h} = P_{bat,max} * 1 \text{ h} = 15,839.76 \text{ kWh} \quad (3.11)$$

However, in order to take current developments in battery technology into account (see section 2.6), a higher power LIB storage with a C-rate of 2 is also investigated. An LTO storage with even higher C-rates is not considered for this analysis since reliable cost information is not available and references of utility scale systems don't exist. The battery capacity of this 0.5-h storage $C_{bat,0.5h}$ is determined through Equation (3.12).

$$C_{bat,0.5h} = P_{bat,max} * 0.5 \text{ h} = 7919.88 \text{ kWh} \quad (3.12)$$

Inefficiencies during charging, storing and discharging are combined into a single efficiency factor of 90 % [10, 67], which is applied to the charge power. Hence no further losses are considered during discharge and the energy stored is fully retrievable.

Since lifetime assessment of batteries is a highly complex topic [73] and accurate calculations, taking the specific utilisation into account, exceed the scope of this thesis, a simplified lifetime model is chosen. For this, a lifetime of 15 years is assumed in which no ageing takes place [67, 74]. After these 15 years the battery system has to be replaced, costing another 30 % of the initial investment [67]. The investment costs for both storages are extrapolated from [75-77], using the moderate scenario for 2023. The green values in Table 3.2 are extracted from the aforementioned sources and converted to Euro using a factor of 0.9. Using the fact that the prices appear to scale linearly with the storage duration, the missing values for shorter durations (higher C-rates) of the commercial and utility scale storages are extrapolated, and marked blue. Finally, since the size of the designed storage is between the two references, the prices are interpolated (purple values). This time a logarithmic progression is assumed. Equations (3.13) and (3.14) show the interpolation of the CAPEX for the 1-h storage. The indexes *com* and *uti* refer to the commercial and utility scale reference storages respectively.

$$X = \log\left(\frac{P_{bat,1h}}{P_{com}}\right) * \frac{\log\left(\frac{CAPEX_{uti,1h}}{CAPEX_{com,1h}}\right)}{\log\left(\frac{P_{uti}}{P_{com}}\right)} = -0,2295 \quad (3.13)$$

$$CAPEX_{bat,1h} = 10^X * CAPEX_{com,1h} = 548.1 \frac{\text{EUR}}{\text{kW}} \quad (3.14)$$

Table 3.2: Battery CAPEX for different storage durations and powers in 2023. Values taken from [75-77] in [USD/kW] and converted to [EUR/kW].

Storage power [kW]	Storage duration [h]					
	0.5	1	2	4	6	8
600 (commercial)	847.42	929.64	1094.08	1422.95	1751.83	2080.71
15,839.76	431.05	548.1	773.26	1208	1634.35	2057.08
60,000 (utility scale)	327.41	442.08	671.43	1130.14	1588.84	2047.55

Operating costs are assumed to be 2 % of the CAPEX per year [60, 67] and are listed in Table 3.3 together with all other relevant characteristics of the storage system.

Table 3.3: Characteristics of the storage system

	Parameter	Value
General	Technology	Li-ion battery
1-h storage	C-rate (CR)	1
	Capacity ($C_{bat,1h}$)	15,839.76 kWh
	Power ($P_{bat,max}$)	15,839.76 kW
	Efficiency (η_{bat})	0.9
Economics	Lifetime (L_{bat}) [67, 74]	15 a
1-h storage	Investment costs ($CAPEX_{bat,1h}$) [75-77]	548.1 EUR/kW
	Operating costs ($OPEX_{bat,1h}$) [60, 67]	10.96 EUR/kW/a
General	Technology	Li-ion battery
0.5-h storage	C-rate (CR)	2
	Capacity ($C_{bat,0.5h}$)	7919.88 kWh
	Power ($P_{bat,max}$)	15,839.76 kW
	Efficiency (η_{bat})	0.9
Economics	Lifetime (L_{bat}) [67, 74]	15 a
0.5-h storage	Investment costs ($CAPEX_{bat,0.5h}$) [75-77]	431.05 EUR/kW
	Operating costs ($OPEX_{bat,0.5h}$) [60, 67]	8.62 EUR/kW/a

3.1.3. Nowcasting system

The nowcasting system itself isn't simulated and thus no parameters are needed as inputs. Solely the costs and lifetime are necessary for the economic analysis in post processing. The lifetime is set to 15 years which corresponds to the expected lifetime of the all sky imagers. Investment costs are estimated, considering the cameras, electrical equipment, a computer, installation and software costs. It is assumed that the PV plant is already equipped with meteo stations and scaffolding to install the ASIs. Applying the same assumption as for the storage system, reinvestment costs after the end of the expected lifetime are set to 30 % of the original costs [67]. During operation the cameras need frequent cleaning. To estimate the associated expenses, a technician's labour costs for ten minutes per day are used [78].

$$OPEX_{NC} = \frac{1 \text{ h}}{6 \text{ d}} * 365 \frac{\text{d}}{\text{a}} * 23.5 \frac{\text{EUR}}{\text{h}} \approx 1430 \frac{\text{EUR}}{\text{a}} \quad (3.15)$$

Table 3.4 shows the implemented values.

Table 3.4: Characteristics of the nowcasting system

	Parameter	Value
Economics	Lifetime (L_{NC})	15 a
	Investment costs ($CAPEX_{NC}$)	25,000 EUR
	Operating costs ($OPEX_{NC}$)	1430 EUR/a

3.2. Configurations

Configurations are combinations of the introduced components. They represent the setups that are investigated and compared against each other.

A total of four different main configurations are considered in this thesis:

- The accordingly named **“Base case”** serves as a base line and validation for the other configurations to compete against. It consists of only the PV system and directly feeds the power output to the grid. It should be noted however that inverter curtailment is used to prevent up ramps in the output power to facilitate a fair comparison against the other setups that make use of this feature (see section 4.3.1. for more details)
- **“Storage”** combines the PV system with a large BESS and compensates all ramps by charging and discharging the battery.

- The **“Nowcast”** configuration trades the BESS for a nowcasting system and uses the predictions to smooth the power output.
- **“Hybrid”** makes use of both a BESS and a nowcasting system. Compared to “Storage” the BESS can be of smaller power and capacity.

These main configurations are further divided depending on the implemented power control strategy (see section 4.3.1) and the specification of the storage system.

3.3. Regulations

A framework of regulations complements the configurations and completes the definition of the use cases. These regulations have to be adhered to by each configuration. In case of violations, a penalty scheme is applied.

3.3.1. Ramp rate limit

In order to limit the fluctuations in the output power, a ramp rate limit is introduced. Following current implementations (section 2.4) and the state of the art in research [9, 11-13, 79-81], this limit is set as a percentage of the maximum power per minute. Not many clarifications exist on how ramp rate measurement and calculation is to be performed [7, 82]. However, [82] lists and visualizes different options (Figure 3.2).

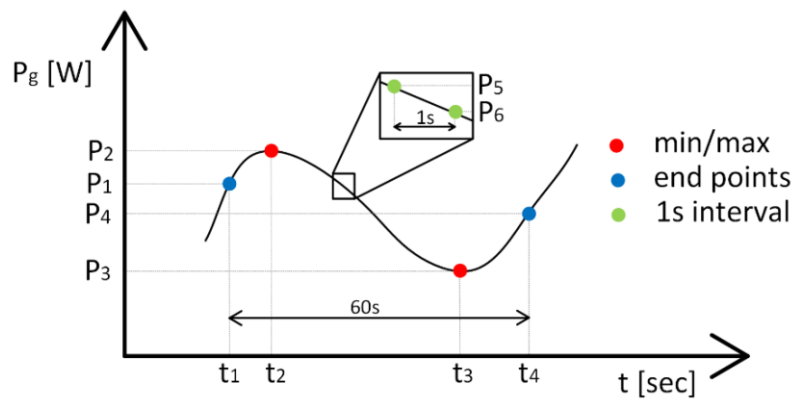


Figure 3.2: Ramp rate calculation methods: difference between two endpoints of a 60-second interval $r = (P_4 - P_1)/(t_4 - t_1)$, difference between the minimum/maximum values of a considered interval $r = (P_3 - P_2)/(t_3 - t_2)$, difference between two points at each second interval $r = (P_6 - P_5)/1\text{ s}$, taken from [82]

The ramp rate is assumed to be monitored by the TSO and thus measured at the grid connection point of the PV plant. The AC power output can be observed and checked for ramp rate violations by one of the methods shown in Figure 3.2. For this analysis,

the end points method with an interval length of 60 seconds is chosen because of its straightforwardness. In practice this means that the observed output power of any given time step simply has to be compared to the output power one minute before. Using Equation (3.16), these two values are computed into a ramp rate r in [%/P_{PV,max}/min] [48] (from now on just written as [%/min]).

$$r = \frac{P_4 - P_1}{P_{PV,max} * 1 \text{ min}} \quad (3.16)$$

Limited by the temporal resolution of the simulation, this calculation is carried out every 30 seconds.

The ramp rate limit that should not be exceeded is set to 10 %/min, following current implementations (section 2.4) and the state of the art in research [9, 11-14, 79]. Every ramp rate measurement that does exceed this limit, either in the up or down direction, is considered a violation. For the sake of simplicity ramp rate violations will from this point on simply be referred to as ramps. Power changes below the ramp rate limit will generally not be called ramps.

3.3.2. Penalties

Ramp rate violations need to be penalized in order to incentivize measures to comply with the limits and smooth the output power. Since implemented penalty schemes are scarce, two different methods are developed, loosely following [37] and [48] respectively.

Fee

Inspired by [37] this penalty scheme implements a fee, which has to be paid for all ramps. The total fee is a function of the amount of energy that was fed in too little in order to adhere to the ramp rate limit. Figure 3.3 visualizes the calculation of the missing energy. First, in order to quantify the severity of a violation, the difference between the actual output power and the closest power within the limits is calculated. This value is higher for more extreme violations. Multiplying the power difference with the time until the next change in the power output, yields the missing amount of energy. The resolution of this calculation is related to the resolution of the power output which itself relies on the frequency of nowcasts. In the case of this study, the time steps are 30 seconds and the power output is assumed to be constant in between.

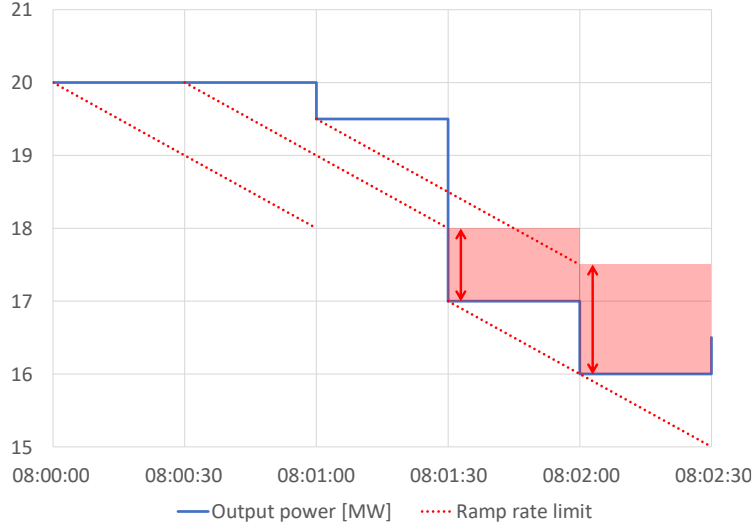


Figure 3.3: Visualization of ramp rate violation energy calculation. The blue line represents the actual power output. The end points of each dotted line show the lowest permitted power, defined by the output one minute ago and the ramp rate limit. The red arrows show the amount of lacking power at a given time step and the bright red areas the amount of missing energy until the next time step.

The missing link for getting from the ramp rate violation energy E_{NC} (NC referring to non-compliance) to a monetary fee is the penalty factor p_{fee} . This factor's unit is [EUR/MWh] and its value determines the number of ramps that is bearable for an economically viable use case, with higher values incentivizing more investment into ramp rate reduction. Equation (3.17) shows the final calculation of the penalty costs C_p .

$$C_p = p_{fee} * E_{NC} \quad (3.17)$$

Non-compliance tax

Instead of a fixed fee, the Puerto Rico Electric Power Authority proposed to observe the ramp rate non-compliance of a plant and implement curtailment penalties as a function of this non-compliance [48]. The proposal is adapted so that instead of the power output, the earnings of the generator are curtailed in the form of a flexible tax. This has the benefit of not reducing the amount of renewable energy fed into the grid while still incentivizing compliance. Additionally, challenging conditions, which often lead to many missed ramps, also often entail lower earnings in general, making the penalties less severe in those cases.

The first step to setting the tax is calculating the non-compliance factor NC . Counting all time steps n_{NC} where a violation has been observed and comparing it to the total amount of time steps n_t within the observed period gives the percentage of non-compliant measurements (Eq. (3.18)).

$$NC = \frac{n_{NC}}{n_t} \quad (3.18)$$

Since this percentage is usually below or around 1 %, the non-compliance factor is then multiplied with a linear factor p_{tax} for scaling, resulting in the final tax factor TF (Eq. (3.19)). Multiplying with the profit R generated in the period gives the amount of the penalty costs C_p (Eq. (3.20)).

$$TF = p_{tax} * NC \quad (3.19)$$

$$C_p = TF * R \quad (3.20)$$

The observation time period is set to one week, therefore balancing different weather conditions [48].

As with the fee penalty scheme, the linear factor p_{tax} can be set to certain values in order to achieve the desired compliance rates.

4. Methodology

This chapter aims to introduce and explain the methods and concepts used in the analysis. Similar to the workflow pictured in Figure 4.1 it is structured in three consecutive parts. The preprocessing section describes the input data and preparation steps necessary to obtain suitable inputs for the simulation. The main focus lies on the generation of validation irradiance maps from point measurements and the calculation of GTI maps for both, the validation and nowcasting data. In the subsequent section, the adjustments made to the state-of-the-art version of the simulation tool are outlined. Finally, in the third section, the postprocessing of the power nowcasts passed from the simulation is described. It is divided into explanations of the control algorithms, the marketing strategy and the economic analysis.

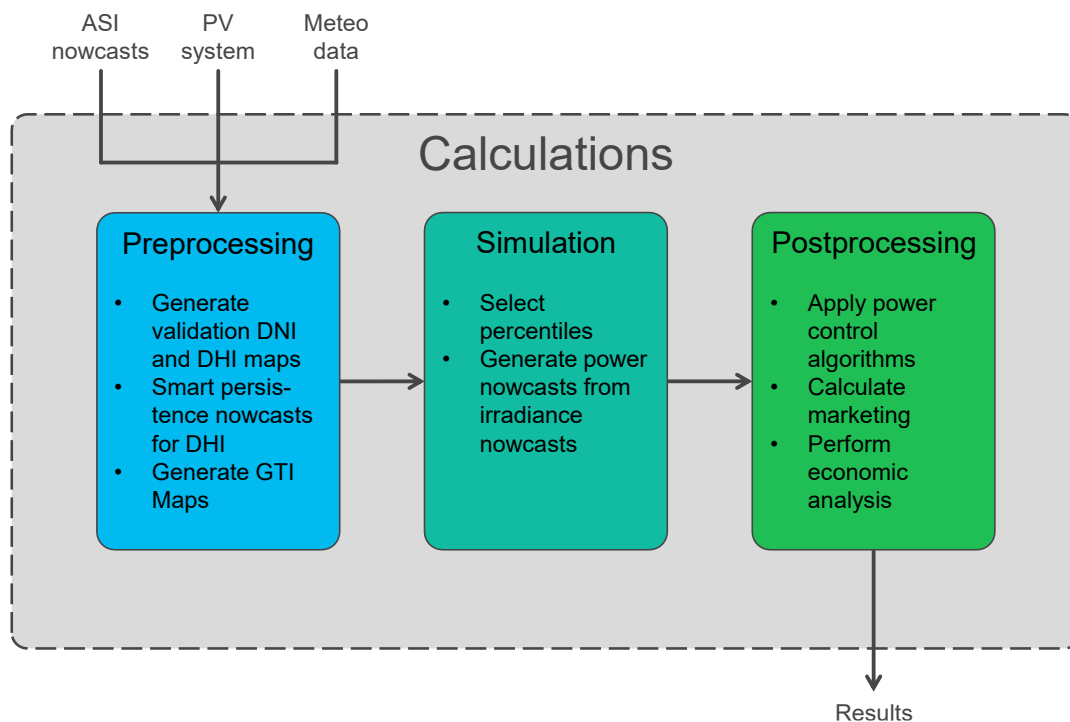


Figure 4.1: Workflow schematic of the calculations and processes carried out. The inputs are fed into preprocessing, the first of three calculation steps. The simulation is a necessary intermediate step, before the final results are generated in postprocessing.

4.1. Preprocessing

The goal of preprocessing is to turn the raw input data into inputs suitable for the simulation. As shown in Figure 4.1, the three main inputs are the nowcasts, information about the PV system and measurements from meteo stations. Each of these input datasets is processed individually with some cross dependencies. In the following, the inputs are defined in greater detail and the executed calculations and modifications are described.

Meteorological data

Meteorological data is obtained from eight meteo stations distributed across the PSA (Figure 3.1). It consists of DNI and DHI measurements as well as temperature, pressure and wind speed data with a resolution of 1 min. While the irradiance data is available for all eight stations, the remaining ambient conditions are only measured at two stations.

The objectives of preprocessing the meteorological data are twofold. One is the provision of a dataset with the current ambient conditions (temperature, pressure and wind speed) at every time step. The second is the generation of a validation set of irradiance maps, containing the current irradiance conditions across the PV plant at every time step. Both are used as inputs for the simulation.

Before processing them, the measurements are filtered for faulty readings and outliers. Ambient temperature, pressure and wind speed are assumed homogeneous across the PV plant area. Thus, only the output of one meteo station is used for most of the time. The output of the second station is only utilized for missing time steps. In case both stations didn't generate a valid measurement, interpolation is used in order to produce a continuous dataset. However, this happens very rarely and only for a single digit amount of consecutive time steps. The final result is the desired dataset of the ambient non-irradiance conditions for the complete time frame.

Knowing the coordinates of the nowcasting grid points, the filtered DNI and DHI measurements of the eight meteo stations are plotted onto the same grid using the "nearest" approximation. Specifically, this means that for each grid point the algorithm checks which meteo station is nearest and takes that value. Inter- or extrapolation is not utilized since it would generate unrealistic scenarios. A slight Gaussian filter is applied to smooth transitions. Figure 4.2 shows an example of a generated DNI map. These so-called validation maps depict the supposedly real irradiance conditions experienced by the virtual PV power plant, which remain unknown to the control systems until the time of occurrence. In this specific example the right side of the plant is shaded, while the left side still receives direct irradiance. Note that the actual shadow border can be anywhere between the stations and must not look like shown in Figure 4.2. The achievable resolution of the modelled spatial

irradiance distribution ultimately relies on the temporal and spatial resolution of the available reference measurements. Since not all stations provide a valid measurement at all times, the three outer stations are included in the nearest approximation in case of unavailability of the central stations.

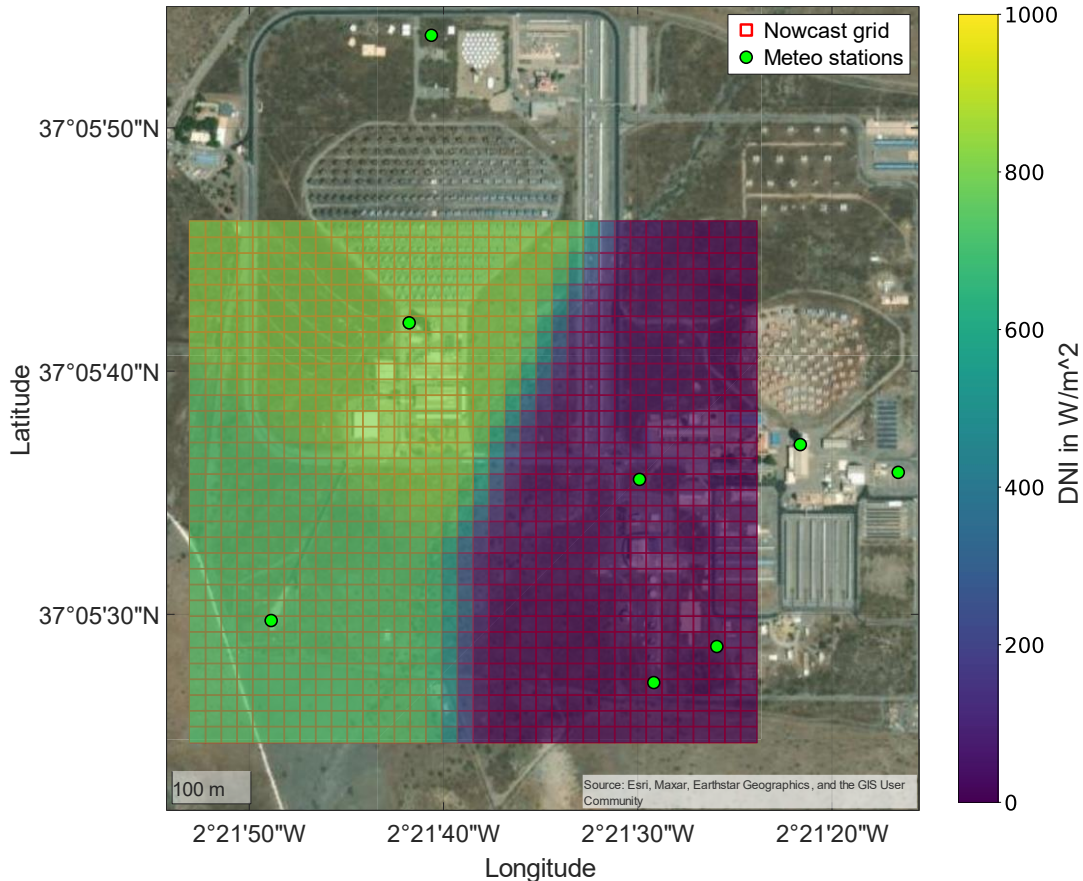


Figure 4.2: Example of a DNI validation map generated from measurements at the meteo stations

By utilizing data on the PV plant's location, orientation and surface albedo, the DNI and DHI maps are processed into GTI maps according to [83] and [84].

The final set of validation irradiance maps is used to calculate the actual power output of the PV plant and therefore represents the conditions that the nowcasts are trying to predict as precisely as possible.

PV system

The PV system has been defined in great detail in section 3.1.1 and the characteristics listed in Table 3.1 are taken as input data.

The only necessary preprocessing consists of the compilation of a list of the exact geographic coordinates of each PV module and the notation of the inverter it is connected to. This information is later used to assign the modules to the correct grid points of the irradiance maps and get the realistic cumulated power for each inverter.

ASI nowcasts

The state-of-the-art generation of the ASI nowcasts has been introduced in section 2.5. For this particular analysis the nowcasts have been created for a 33 x 36 grid overlaid over the area of the virtual PV system, providing a spatial resolution of 20 m (see Figure 3.1). Each grid point corresponds to one DNI value. The utilized ASIs at PSA are also shown in Figure 3.1. A nowcast for a single time step comprises five probabilistic maps corresponding to the percentiles P10, P20, P30, P40 and P50 for each lead time. In this case eleven lead times are used as inputs, namely LT0 – LT10. These 55 irradiance maps are generated for every 30 seconds of the chosen one-year time frame from 2020/09/01 until 2021/08/31 (only at daytime). Excluding six days where availability issues occurred, nowcasts for 359 days (making up a total 459,607 time steps, 25,278,385 irradiance maps and $\sim 30 \times 10^9$ DNI values) are used as input data for the preprocessing.

First, these DNI nowcasts are filtered to exclude time steps with sun elevation angles of less than 2.5° . These time steps are error prone while of almost no relevance for the power generation. The resulting start and end times of each day are noted and define the time frames used in the simulation.

In order to generate GTI nowcasts in the same way as done with the validation maps, the DNI nowcasts need to be accompanied by DHI values. Since no ASI nowcasts exist for the DHI, a “smart persistence” nowcast is created. This smart persistence nowcast only takes one measurement of the current DHI, assumes persistent ambient conditions and generates a prediction of the future DHI, only considering changes in the sun elevation. Subsequently, the GTI nowcasts are calculated from the DHI and DNI nowcasts according to [83] and [84].

The only missing input for the simulation is the information on variability classes (see Table 2.2). Similar to the nowcasts, this is available as a set of the current class and the predicted classes for each time step.

4.2. Simulation

The basic structure of the simulation tool has been introduced in section 2.7. This section describes the changes that are performed in order to adapt to the new requirements.

Following the flowchart in Figure 2.5, no adaptations are necessary in the sub-system “Irradiance Analysis”. The “MIX” strategy for selecting the nowcasting percentiles based on the variability classification, introduced by [16], is kept unchanged.

In “PV Array” several performance optimizations are carried out. Filtering of duplicate irradiance conditions and vectorization of the detailed calculations for the PV modules bring down the amount and time requirement of the computations significantly.

Additionally, the correction factors of the PVWatts inverter model are updated. All factors presented in [65] are implemented. The only exemption is the shading factor, since it is accounted for by the irradiance measurements. While the soiling factor is multiplied to the irradiance values, all other factors are applied onto the DC power calculated in the “PV Array” sub-system. More details about the calculations and a comprehensive flowchart are given in [16] and [85].

The previously following “Output Power Control” and “Storage” sub-systems are removed and added to the postprocessing (see section 4.3) in order to save complexity and gain flexibility.

On the system level scope additional major runtime improvements are achieved through multiprocessing and the replacement of the lead time 0 nowcasts with the validation data. The latter skips the unnecessary calculations of lead time 0 since it is not used in the subsequent power control.

Using the validation irradiance maps as inputs yields the actual prevailing power output of the PV plant which is consequently referred to as validation power. The nowcasted irradiance maps are processed into nowcasts of the power output.

All performance improvements combined enable the simulation tool to process the much larger dataset of one year with 30 second time steps (compared to 18 days with 1-minute time steps in [16]) in a much more reasonable time.

4.3. Postprocessing

The postprocessing is responsible for dealing with the power nowcasts generated by the simulation. The first step is to create a power output by applying a control strategy. These strategies set the output power with respect to the grid regulations, limitations of the available hardware (e.g. the storage system) and the information provided by the nowcasts. Afterwards, the energy is marketed and a monetary value derived. Finally, the results are fed to the third stage, which is the economic analysis of the system. Each step is explained in greater detail in the following sections.

4.3.1. Power control strategies

The general structure of the power control is visualized in Figure 4.3. The program receives all power nowcasts, the curve of the actual prevailing (validation) power output of the PV plant, as well as parameters, which define the details of the configuration (chapter 3) and set the strategy.

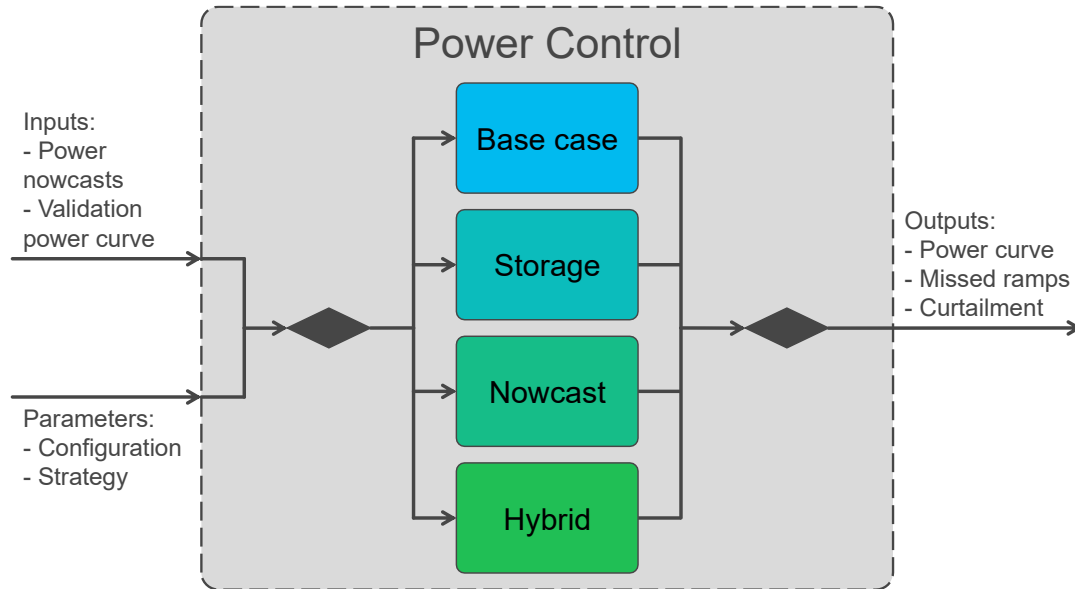


Figure 4.3: Power control with selection of strategies and associated inputs and outputs

Corresponding to the main configurations introduced in section 3.2, the strategies are divided into four main cases: base case, storage, nowcast and hybrid. The latter two are further subdivided depending on the nowcasting algorithm.

The power control module selects the correct control strategy and passes the inputs one time step at a time. After the algorithm produces its outputs, the power control collects and combines them. This results in a power curve of the system power (the power that is actually fed into the grid) and information about missed ramps and curtailment.

The following sections describe the respective power control strategies in detail.

Base case strategy

The base case operates under a fairly simple principle (see Figure 4.4). Since no nowcasts exist in this configuration, the base case can only react to the validation power that is generated by the PV system at any particular moment. This and the fact that a storage system isn't available either, means that sudden down ramps of the PV power are directly passed to the grid and can't be smoothed. However, the situation

is different for up ramps of the PV power. Due to the presence of an active power controller (see section 3.1.1), the PV power can be curtailed by the inverters in such a way that the system output does not violate the ramp rate limit. In the algorithm this is achieved by comparing the output of the current time step with the previous one. In case a violation is detected, the output is reduced to stay within bounds and the difference between generated PV power and fed-in system power is noted as curtailment. This system works for 100 % of the up ramps and thus the final count and energy amount of the missed ramps only consists of downward ramp violations.

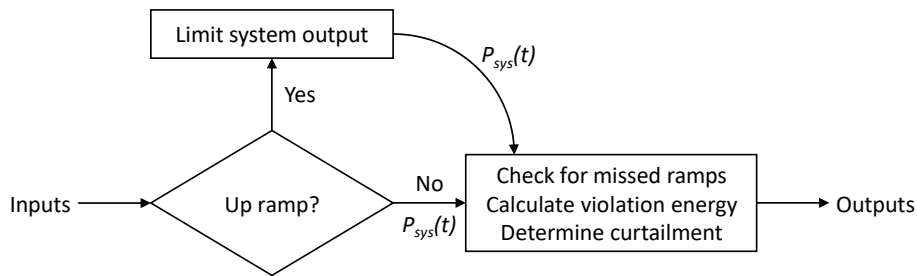


Figure 4.4: Flowchart of the base case power control strategy

Storage strategy

Still missing a nowcasting system, the storage strategy also can only react to the actual power generation of the PV system. The difference however, is the ability to deal with both, up and down ramps. Figure 4.5 shows a simplified flowchart of the algorithm.

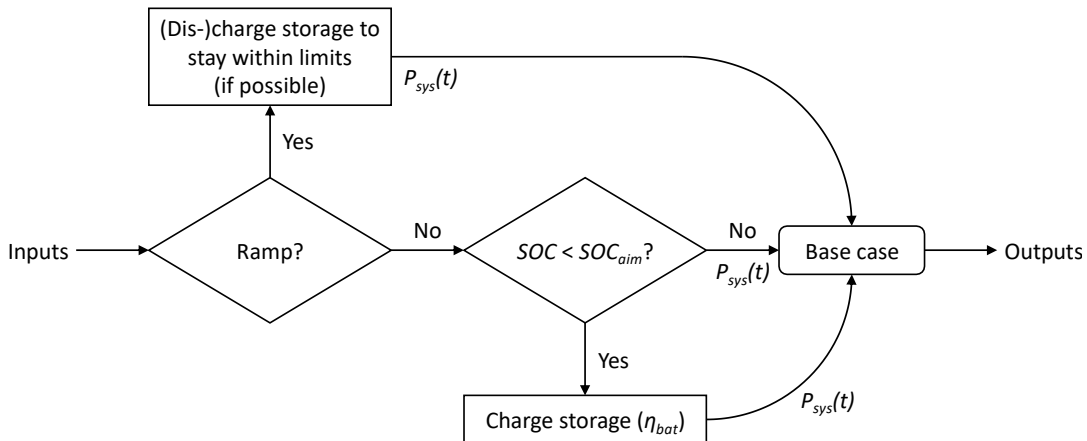


Figure 4.5: Flowchart of the storage power control strategy

If a ramp is detected when comparing the current validation power against the previous system output, the battery is either charged or discharged, depending on the sign of the ramp. During this process, the current SOC of the battery is continuously

monitored, and the system considers the restrictions on charge and discharge capabilities based on the SOC or the maximum power specifications. Further, the battery efficiency is applied on each charge cycle, reducing the amount of energy that is actually being stored and can be retrieved later. In case no ramp is present, a second check is performed, examining whether the current SOC is below the goal (50 % by default). If the check returns true, the storage is charged, reducing the system output in the process. Otherwise no adjustments to the PV power need to be made. Whichever way it is calculated, the resulting system power of this time step is passed to the base case module. In it, a second up ramp detection and mitigation is performed (important if the battery is at 100 % SOC) and the gradient and curtailment of the final output is analysed.

It is important to note that the storage is not discharged if the SOC is above the targeted SOC and no ramp is present. This is due to increased imbalance costs caused by larger deviations from the validation power (see section 4.3.2 for further information). In order to restore the SOC to its default value at the end of the day, the excess (or missing) energy is sold (or bought) at night (refer to section 4.3.2).

Further, the storage is not used for any service other than ramp rate mitigation. It also does not keep track of the imbalance caused in the current 15-minute settlement period and does not charge or discharge accordingly to minimize the final imbalance payment.

Lastly, the battery is unfortunately unable to store the energy that is curtailed in the inverters during very high irradiances and subsequent exceedance of their maximum DC power rating. This is a result of the power control being based on the AC power output of the PV plant.

Nowcasting strategies

The nowcasting system enables the control algorithm to use predictions in order to mitigate not only up but also down ramps without the use of a storage system. A simplified flowchart of the algorithm is presented in Figure 4.6 and will be explained in the following.

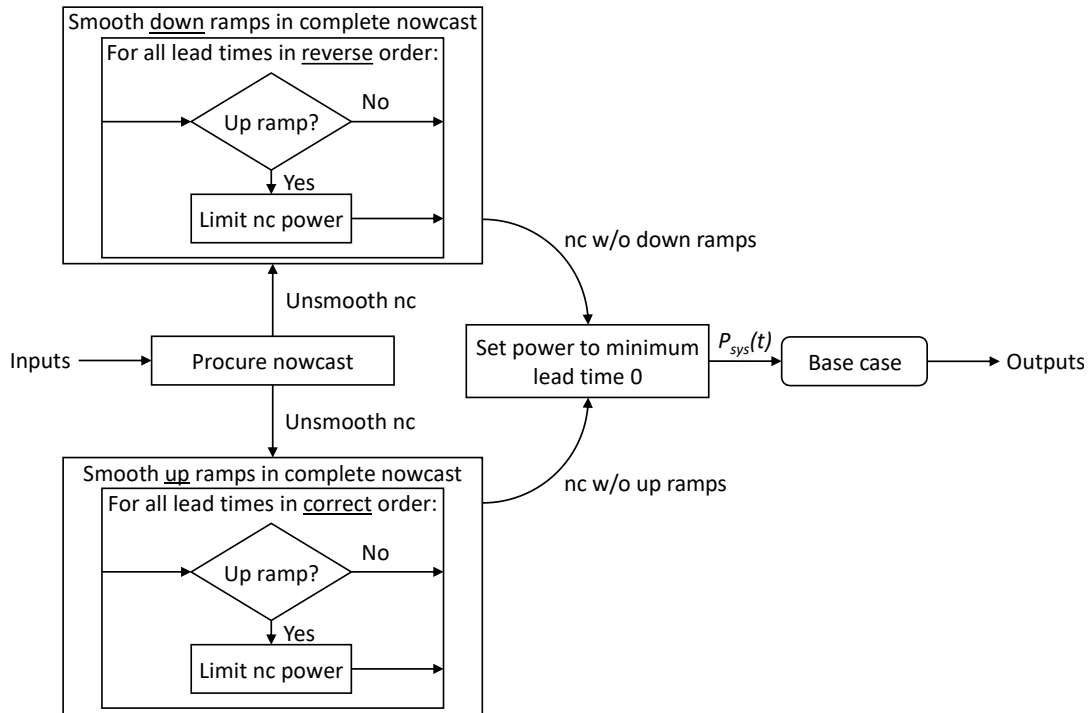


Figure 4.6: Flowchart of the nowcast power control strategy

Four different nowcasting strategies are developed and investigated in this work. They all share the same structure and only differ in the very first step, the procurement of the nowcast.

- **“Last”** is the most intuitive strategy. Here, the nowcast used for the control is only the most recent one. Because of this, it is the most accurate prediction of the upcoming conditions and lead time 1 of the nowcast corresponds to the expected power output one minute from the current time step. This forecasted power curve of the following ten minutes is then passed on to the next steps. However, since the accuracy is still far from 100 %, many ramps are going to be missed by this strategy.
- **“Min”** is a more conservative approach. Instead of only taking the current nowcast, all nowcasts of the previous ten minutes are considered. The result is a range of differently aged nowcasts for each of the upcoming time steps. For example, the output one minute into the future has an LT1 prediction from the current nowcast, an LT2 prediction from one minute before and so on all the way to an LT10 prediction from nine minutes before. The amount of different predictions shrinks for time steps further from the current one. As the name suggests, the “Min” strategy looks at all predictions for each future time step and selects the smallest one, resulting in a power curve with

all the lowest estimates. While this strategy is going to catch a lot more ramps, there is also going to be a lot of unnecessary curtailment due to too low estimates.

- A way of reducing the curtailment caused by wrong low predictions is introduced with the **“Mean”** strategy. It works in the same way as “Min” in the sense of collecting previous nowcasts but instead of looking for the minimum, the average of all predictions is calculated for each future time step. Both, the “Min” and “Mean” strategies give all nowcasts the same weight, disregarding the fact that higher lead times are less accurate (as later shown in section 5.1).
- Which is where the **“Weighted”** strategy aims to improve. In it, each lead time is multiplied with a factor depending on its typical accuracy, before taking the average. This results in a power curve where for each time step all previous estimates are considered but the most recent one is weighted stronger than one from several minutes before. The factors used are derived from the continuous ranked probability score (CRPS) of the different lead times of the nowcasting system in use at CIEMAT’s PSA and are listed in appendix B. The CRPS has been determined over the course of 93 days [53].

In order to analyse the theoretical potential of nowcasting, the “Nowcast” configuration is also studied with an ideal input. Ideal referring to a perfect nowcast which accurately predicts the exact future irradiance and acts as the limit increasingly powerful nowcasting systems can approach but never reach. The procurement step of this “Ideal nowcast” strategy simply reads the validation powers for the following ten minutes, effectively looking into the future, and passes them to the next steps.

Another part of the procurement of the nowcast for a certain timestep is interpolation. Since the nowcasts are generated every 30 seconds, the power control is performed in this frequency. However, each nowcast only provides power forecasts with a temporal resolution of one minute. To solve this discrepancy, the half minute lead times are linearly interpolated.

Depending on the irradiance conditions, the procured power nowcast features ramp rate violations. In order to find a power curve that complies with the ramp rate limit and set the current output power accordingly, the nowcast needs to be smoothed. While Figure 4.6 shows the general flowchart, Figure 4.7 provides an exemplary set of interim results of this crucial process for a better visualization.

The smoothing is done in two separate modules. One is adjusting the power for each lead time in such a way that no up ramps are present anymore and the other does the same for down ramps. The modules operate by iterating through the nowcast,

comparing the power of the current lead time with the one before and adjusting the current one if necessary. Since the down ramps can only be solved via curtailment in the time steps prior, a forward iteration would detect the ramp at a point where it is too late. That's why for mitigating down ramps, the iteration across the lead times is performed in reverse and up ramps (which are down ramps in reality) are detected and removed through curtailment.

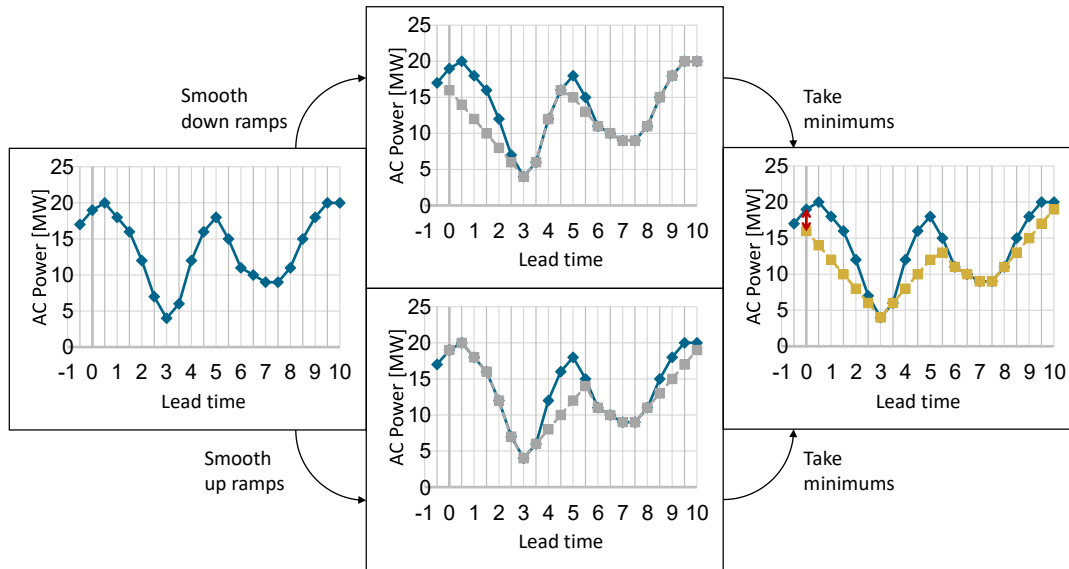


Figure 4.7: Exemplary interim results of the nowcast smoothing process. Each graph shows an exemplary result of the corresponding step in the flowchart in Figure 4.6. The blue line represents the procured nowcast, grey corresponds to the partially (either up or down) smoothed nowcasts and yellow shows the combined and fully smoothed result. The red arrow depicts the ordered curtailment for the current time step.

The two resulting power curves, one without up ramps, one without down ramps are combined into a single power curve containing neither up nor down ramps by taking the minimum for each lead time. Subsequently, the final value for lead time 0 is set as the system power of the current time step. In case no ramps are detected, the system power is set to the maximum value allowed by the previous output and the available validation power. It should be noted that the power is always set for the current time step, meaning the generation and preparation of the nowcast, the control algorithm and the settling of the output power is all assumed to be instantaneous. Lastly, the final system power is passed to the base case module, where it is analysed for ramps and curtailment. The second ramp detection is in this case redundant and has no influence on the result.

Hybrid strategies

Although advanced control strategies with a combined utilization of forecasts and a storage system have been described in literature (e.g. [13]), these strategies rely on very accurate forecasts and their implementation exceeds the scope of this thesis. Therefore, the hybrid strategy is interpreted as a nowcasting strategy appended with a storage system and implemented accordingly. Figure 4.8 shows the simplified flowchart.

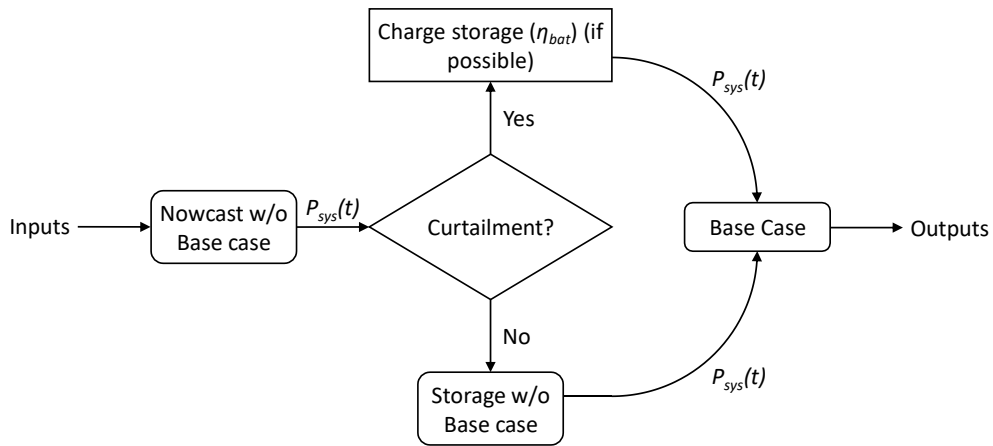


Figure 4.8: Flowchart of the hybrid power control strategy

First, the previously described nowcasting module is called and the proposed system power is read, skipping the further processing in the base case module at this stage. This system power is compared against the validation power at the current time step in order to determine whether the recommendation implies curtailment. If so, the curtailed power is fed into the storage as far as SOC, maximum power and efficiency allow. While the system power remains the same in this case, the otherwise curtailed energy can be fully or partially stored and be used or sold at a later time. In the case of no suggested curtailment, the storage module is called. In it, either a potential ramp that has not been mitigated through curtailment in previous time steps is tried to be buffered by the battery or the SOC is adjusted to meet its target. Whichever way the final system power is calculated, it is then passed to the base case module to analyse the output. The final ramp detection is again redundant because of the nowcasting module where up ramps are already ruled out.

The hybrid strategy is set up with all four different types of nowcasting strategies, resulting in very different approaches. The conservative “Min” strategy already catches most ramps. In this case the storage has to perform less ramp rate control and acts more as a means to reduce the very high curtailment. The opposite “Last” strategy entails much smaller curtailment but leaves a very high number of ramps to be dealt with by the storage system.

4.3.2. Marketing strategy

Marketing of electricity is a highly complex undertaking and can't easily be simulated. The success is strongly influenced by the conditions in the grid or market and the ability of the marketer to react accordingly. Further, it is not always trivial to choose the most profitable marketing strategy, since it depends on the available system, the prevailing conditions, available forecasts or may include special contracts and subsidies. Therefore, instead of being as realistic as possible, the main purpose of the implemented marketing strategy is to provide a common baseline, which is reasonably close to real world applications. The aim is to enable a fair and meaningful comparison of different configurations. The core steps of this strategy are shown in Figure 4.9 and are carried out for each individual day.

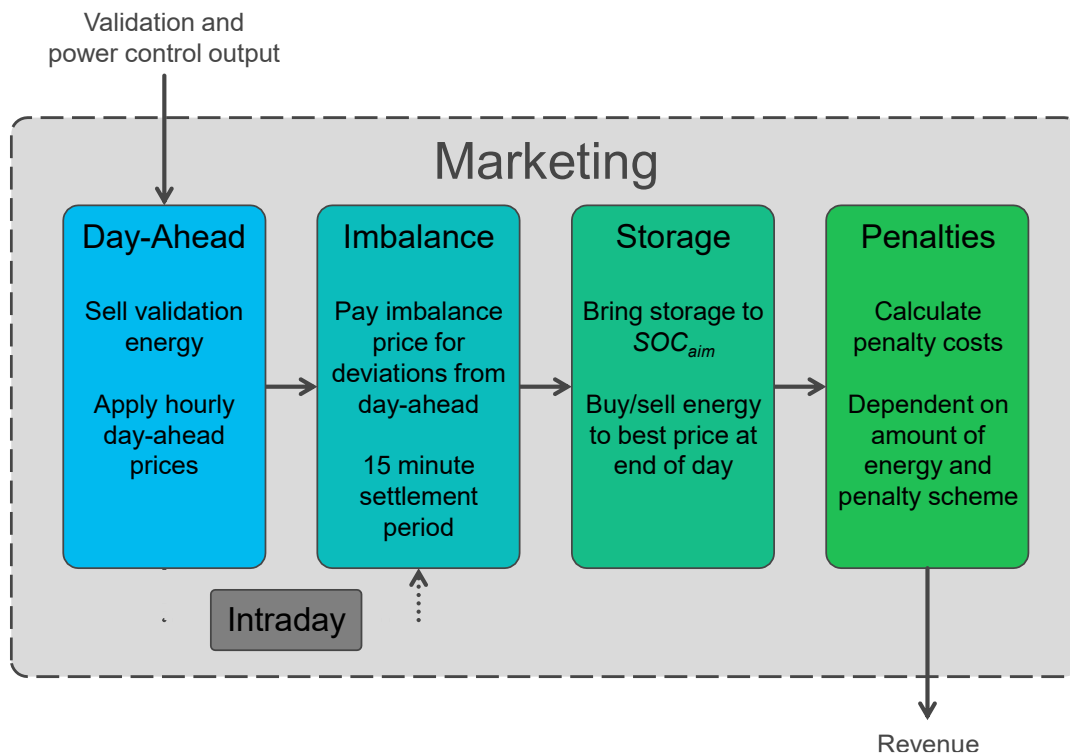


Figure 4.9: Marketing strategy with the sub-modules day-ahead, imbalance, storage and penalties

Being fed the validation data and power control output of a complete day, the first step is the day-ahead marketing. This entails selling the energy on the day before the generation. Since no realistic day-ahead forecasts exist in this scenario, the energy amount to be sold is set to the validation energy, thus assuming the availability of a perfect day-ahead forecast. While this assumption is unrealistic, identical day-ahead

cashflows provide an equal starting point for all configurations and eliminate the influence of this out-of-scope part of the marketing on the final results.

After selling the validation energy amount using the hourly day-ahead prices and storing the generated benefit (positive cashflow), the inputs are passed to the next step. Usually this would be intraday trading, where predicted deviations from the day-ahead trades are sold or bought in order to prevent large differences between traded and actually supplied energy amounts. However, since nowcasts only provide predictions up to 20 minutes into the future and Spain does not possess an intraday market operating at this time scale (see section 2.3), the intraday trading has to be skipped.

Next, the balancing market is emulated. In it the difference between the most recent traded energy amounts (in this case the day-ahead trades) and the actual feed-in is analysed and penalized with the imbalance price. Since no surrounding market is present, the distinction between helping and amplifying imbalances can't be made. Thus, all imbalances are penalized by default and none are remunerated. During the time of data acquisition, the balancing market in Spain operated under a 1-hour settlement period [28]. Consequently, imbalance prices are available in 1-hour time steps. However, recently the system received an update in order to align the market with the rest of Europe and 15-minute settlement periods were introduced [86]. Since this leads to an increase in overall imbalance amounts due to less opportunities to compensate negative with positive imbalance and vice versa, the new 15-minute settlement period is used for the calculations.

Because of the intricacies of the storage strategy (section 4.3.1), the battery is not at its target SOC at the end of most days. Most likely the SOC is higher. In order to restore the SOC to the target before the start of the next day, energy needs to be bought or sold during the night. For a realistic simulation of this process, the prices of the Spanish intraday trading session “22” of the continuous market are consulted. This session is open at the end of the longest simulated days (19:00 – 20:00) and allows trading for the complete night starting at 22:00 [87]. Depending on whether the battery needs to be charged or discharged, the hour with the lowest or highest price is chosen for buying or selling the necessary energy respectively.

Lastly, the missed ramps, more precisely their associated energy amounts determined in the power control module, are used in the penalty calculation, where one of the two penalty schemes (section 3.3.2) is applied.

Appending the formula from [88], the final profit R is calculated according to Equation (4.1) with B_{da} being the benefit obtained from day-ahead trading, C_{imb} and C_p the costs of imbalances and penalties and R_{SOC} the net cash flow generated from buying or selling the deviations from the target SOC at the end of the day.

$$R = B_{da} - C_{imb} + R_{soc} - C_p \quad (4.1)$$

4.3.3. Economic analysis

After the power control and marketing have been performed, the final step in postprocessing is the economic analysis with the generation of the end results. It consists of two main parts, the calculation of the levelized cost of energy (LCOE) and the calculation of the net present value (NPV).

Levelized cost of energy

The LCOE for any given configuration is determined according to Equation (4.2) [89]. As the name suggests, it is a measure for the costs involved in electricity production and depends on the technology used. It is calculated by dividing the overall lifetime costs by the total energy supplied and thus is usually presented in [ct/kWh]. The investment costs I_0 contain the upfront costs of all parts of the system. Depending on the configuration these are PV, storage and/or nowcasting costs. They are calculated by multiplying the CAPEX of the respective system with its size. The second part of the numerator contains all costs that occur during operation. These are just the yearly operating costs of the systems for most of the years. However, since the storage and nowcasting systems have shorter lifetimes than the PV system, they need replacement at their end of life and these expenditures need to be considered in the year they arise in. Taking future cost reductions and reusability of parts of the installations into account, the reinvestment costs are assumed to be 30 % of the original costs [67]. The resulting system costs $C_{sys,t}$ of each year t are discounted with the discount rate i and added up until the end of the PV system's lifetime L_{PV} . Similar to the lifetime costs, the lifetime energy in the denominator is also calculated by discounting and adding up the yearly supplied energy $E_{sys,t}$ for the entire lifetime. Due to the one-year simulation time frame, $E_{sys,t}$ does not change and is assumed constant for all years. Note that because only 359 days are simulated, $E_{sys,t}$ is multiplied with a factor of $\frac{365 \text{ d}}{359 \text{ d}}$ to get the energy for the full year.

$$LCOE = \frac{I_0 + \sum_{t=1}^{L_{PV}} \frac{C_{sys,t}}{(1+i)^t}}{\sum_{t=1}^{L_{PV}} \frac{E_{sys,t}}{(1+i)^t}} \quad (4.2)$$

There's no clear indication whether further costs like penalties are typically part of a system's operating costs and therefore need to be considered in the LCOE calculation. For the purpose of this thesis, two variants are given in the results. One containing only the costs that are directly related to the system in use, thus representing the real

cost of the generation while disregarding any regulations, and the other considering the penalty costs as a part of the operating costs. The first variant is named $LCOE_{np}$ and the second variant $LCOE_p$. Especially the difference between the two is of interest, since it shows the influence of the penalties on a certain configuration and the price such a regulation adds to electricity generation costs.

Net present value

The NPV is essentially the sum of all cashflows during the lifetime of the PV system discounted according to the year they occur in. The formula is similar to the numerator of the LCOE (see Equation (4.3)) [90]. However, instead of just the system costs (reinvestment and operating costs), the yearly profit R_t is also inserted. As shown in Equation (4.1), it includes the rest of the relevant cashflows, namely day-ahead benefits, imbalance and penalty costs as well as cashflow from SOC restoration. Like the yearly supplied energy in the LCOE calculation, the yearly profit is also multiplied with a factor of $\frac{365 \text{ d}}{359 \text{ d}}$ in order to respect the slightly shorter simulation time frame.

$$NPV = I_0 + \sum_{t=1}^{L_{PV}} \frac{R_t - C_{sys,t}}{(1+i)^t} \quad (4.3)$$

The result is returned in Euro and is used to analyse the value of the investment under study. In general, values above zero mean that the investment is more profitable than an investment with an expected rate of return equal to the discount rate i . This is a prerequisite for a viable investment. When comparing two investments against each other, the one with the higher NPV is more profitable and is to be preferred.

Discount rate

The discount rate plays a major role for the calculations of the LCOE and NPV. Its influence on the profitability of the investment is investigated in section 5.4. Generally, the discount rate is set to the weighted average cost of capital (WACC). This value is strongly dependent on the country and the type of investment. The International Renewable Energy Agency (IRENA) examined the WACC for several countries and different renewable energy sources [91]. For utility scale PV systems in Spain a value of 5.1 % is found.

5. Results

The following chapter presents the results of this thesis. It is structured in four parts. First, the output of the simulation tool is shown and analysed. Then, the power control algorithms are benchmarked against each other. Next, the economic analysis is performed, the essential results are compiled and different configurations compared against each other. Finally, to thoroughly explore the impact on the results, a sensitivity analysis is conducted by varying the system parameters.

5.1. Simulation results

The simulation tool takes irradiance data as input and simulates the PV plant. This results in power curves for each of the days analysed. Figure 5.1 shows the output power curve for an exemplary day in blue. The orange and red lines display the DNI and GTI inputs respectively. As to be expected, the power output correlates perfectly with the irradiance inputs, thus demonstrating the reliable processing of the irradiance data to power data by the simulation tool. This example uses the validation irradiance inputs retrieved from measurements (see section 4.1).

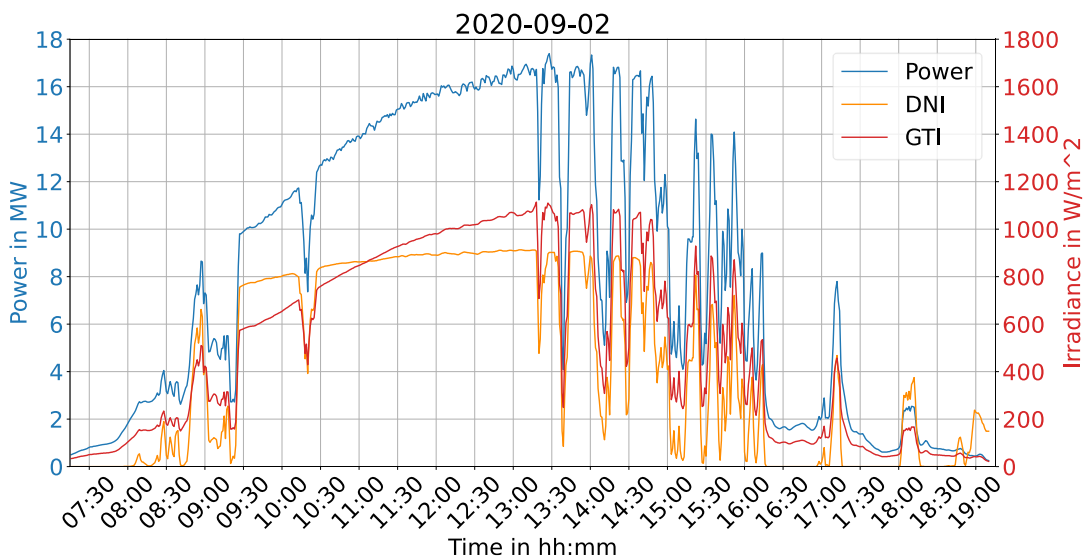


Figure 5.1: Validation irradiance and power curves for an exemplary day

Additional to this validation power curve, similar curves are generated in the same way for each of the nowcasted irradiance conditions. Since no actual reference power data exists as a verification, these power nowcasts can only be analysed by comparing them against the validation power generated from the measured irradiance data and taking note of the deviations. It is crucial to emphasize that the PV model employed in this study was previously validated in [16] using real power data. Hence, the analysis in this study focuses solely on evaluating the forecast accuracy rather than the PV model's performance, which has already been established. The (power) nowcast accuracy is expressed in the three error metrics Bias, root mean square error (RMSE) and mean average error (MAE). Equations (5.1)–(5.3) show the calculation of these metrics [92]. They are evaluated for each day of the year under study with n being the amount of time steps, \hat{y}_i the forecasted power output and y_i the validation power value at time step i .

$$Bias = \frac{1}{n} \sum_{i=1}^n \hat{y}_i - \frac{1}{n} \sum_{i=1}^n y_i \quad (5.1)$$

$$RMSE = \sqrt{\frac{1}{n} \sum_{i=1}^n (\hat{y}_i - y_i)^2} \quad (5.2)$$

$$MAE = \frac{1}{n} \sum_{i=1}^n |\hat{y}_i - y_i| \quad (5.3)$$

In order to obtain a representative output, only the P50 values are utilized for the power validation as they represent a deterministic nowcast. The results are compiled in box-and-whisker plots in Figure 5.2. All three error metrics gravitate to higher values and a higher spread with increasing lead times. Detailed results are given in Table 5.1 for lead times 1, 5 and 10.

Table 5.1: Bias, RMSE and MAE of the AC power of the complete year. Absolute values as well as values normalized to the maximum power are given for lead times 1, 5 and 10.

Lead time	Bias		RMSE		MAE	
	abs. [kW]	max [%]	abs. [kW]	max [%]	abs. [kW]	max [%]
1	6.9	0.03	769.3	3.64	293.8	1.39
5	17.6	0.08	1310.0	6.20	611.5	2.89
10	42.0	0.20	1617.6	7.66	831.2	3.93

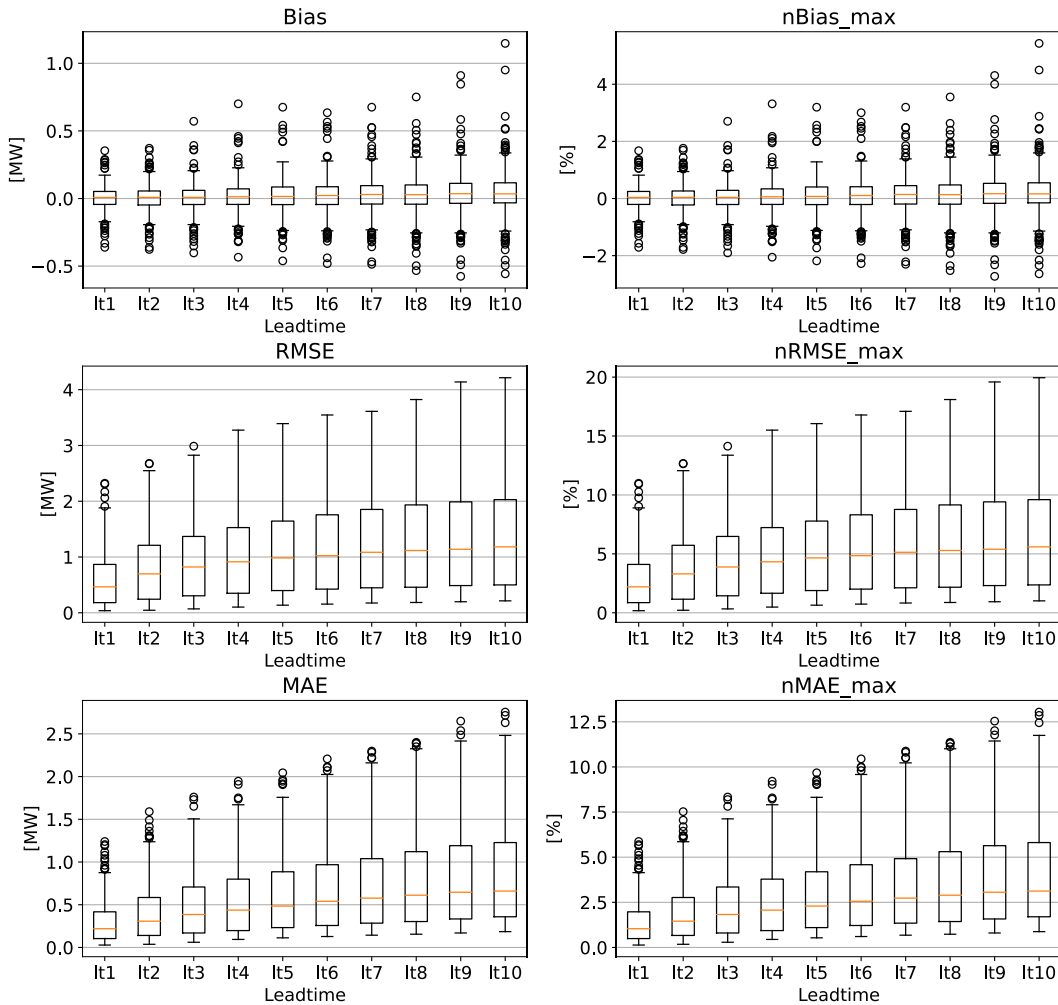


Figure 5.2: Box plots of AC power error metrics. The plots show Bias, RMSE and MAE of the forecasted AC power output compared to the validation output. Broken down for lead times 1 to 10. Absolute values are on the left, percentages relative to maximum power $P_{PV,max}$ on the right. Each plot displays the mean (orange line), the second and third quartile (black rectangle), the 1.5 interquartile range (T-shaped whiskers) and outliers (black circles). Inputs are the P50 error values calculated for each day.

Analysing the results, it appears that the Bias exhibits the smallest spread, with most values close to the median. However, on some days the predictions show a significant deviation, indicated by the black circles marking the outliers. The median Bias is below 0.2 % for all lead times, which attests a very low systematic deviation in the nowcasts. RMSE and MAE have a wider spread and consequently fewer outliers. Their median normalized values are below 7.7 % and 4 % of the maximum power respectively. Overall, the error metrics observed in this work behave similar to the ones observed in [16] and don't show signs of unexpected deviations.

5.2. Power control algorithms

This section benchmarks the performance of the different power control algorithms. First, a single exemplary day is analysed and the strategies are compared against each other. Afterwards, the results of the complete time frame are investigated. For now, the focus lies only on the power-related outputs.

5.2.1. Single day performance analysis

The 2nd September 2020 is chosen for the detailed single day analysis. It contains both, clear sky and clouded conditions and shows a wide variety of important features in the results.

All major strategies (introduced in section 4.3.1) are examined and their power output, and gradients plotted in order to understand their operational methods and analyse the differences between strategies. Although the algorithms technically provide step charts with instant changes at every time step as outputs, the shown graphs contain smooth lines for a better readability.

The first figure (Figure 5.3) compares the base case against the ideal nowcast algorithm. Both of them can't compete against the other strategies since they either don't present a solution for ramp rate mitigation or are unrealistic. Yet they still provide interesting insight in the necessities of ramp rate control and the inner workings of the power control.

In the top graph of Figure 5.3 the power curves of the example day are plotted. Only very minor deviations from the violet validation line by both algorithms are observed. On steep down ramps, such as the one around 13:30, the preemptive curtailment by the ideal nowcasting is visible. Steep up ramps show the curtailment of the base case algorithm (e.g. 14:15). The middle graph gives more detailed information on the curtailment administered by the two strategies. Because of its limited capabilities, the base case only features peaks in the curtailment power when an up ramp happens in the validation power. The ideal nowcast exhibits the same peaks for all the up ramps and additionally shows curtailment for all the downward ramps of that day. Since no storages are present, the curtailment is lost and can't be stored. The effect of this curtailment is shown in the bottom graph. It plots the gradients of the power output at any given time step. While during the first half of the day the validation almost never surpasses the limit of 10 %/min, the early afternoon features lots of ramp rate violations. This is why the majority of curtailment is necessary during this time and almost none is needed in the first half of the day.

Looking at the gradients, both the ideal nowcast and the base case are able to mitigate 100 % of the upward ramps. The downward ramps however are only caught by the ideal nowcast.

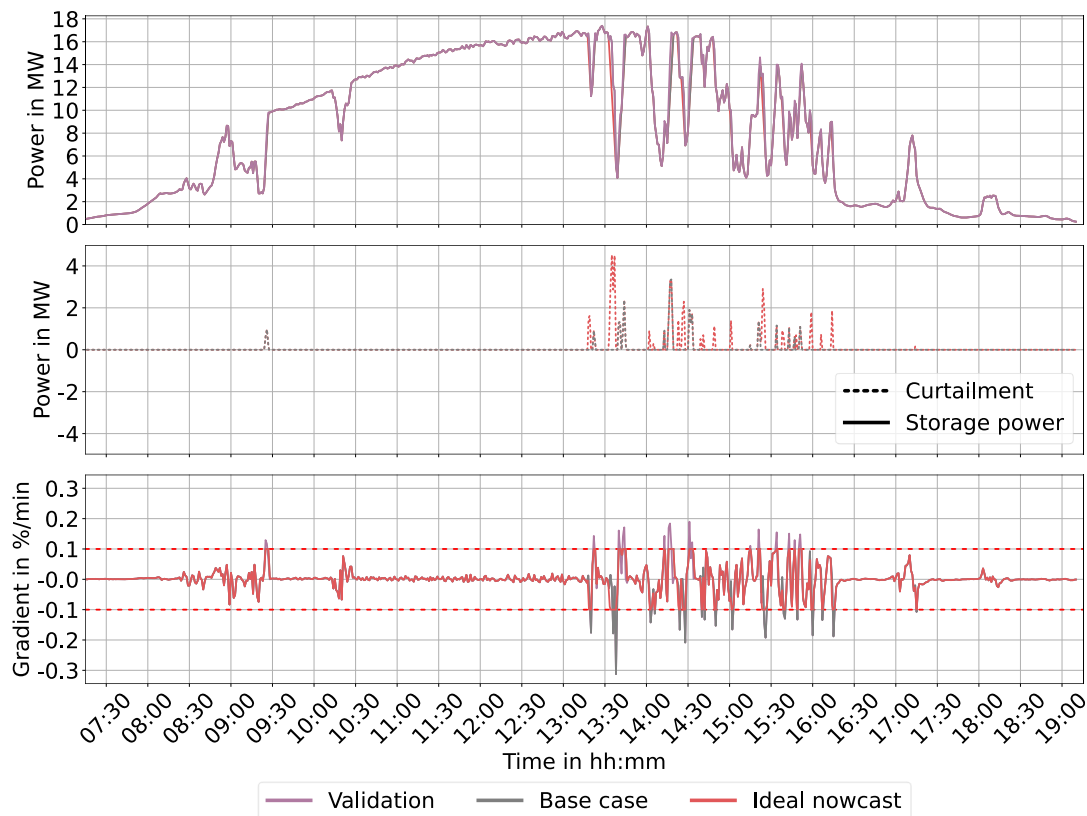


Figure 5.3: Performance charts of base case and ideal nowcast for one exemplary day (2020/09/02). From top to bottom: graph of power output, graph of curtailment (storage power is zero since no storage is present), graph of gradient. The horizontal dashed red lines in the bottom graph indicate the ramp rate limit of 10 %/min.

In conclusion, the results of the base case demonstrate that no further hardware or algorithms are necessary to mitigate all up ramps and thus every other configuration is able to achieve the same. The ideal nowcast shows the theoretical minimum of curtailment required for down ramps, ensuring full compliance with the ramp rate limit.

Since ideal nowcasts are impossible, the next figure (Figure 5.4) presents an analysis of currently achievable (realistic) nowcasts, which are then compared against the storage strategy. Right away it is very obvious that the realistic nowcasting strategies feature a lot more curtailment than the ideal one. Additionally, the different “aggressivities” of the nowcasts are clearly visible in the amount of curtailment. A large portion of this curtailment is unnecessary. One striking example is found at 12:45 where especially the “Min” strategy curtails a lot even though the validation does not contain any ramp. The effects of the different aggressivities are also apparent in the gradient graph. In the first half of the day the “Min” strategy exhibits much higher

gradients than all other algorithms. However, by design it stays within bounds during curtailment. As soon as the validation presents actual ramps, the differences become more pronounced and relevant. Between 14:30 and 16:30 all nowcasting strategies except “Last” are able to mitigate all down ramps. At around 14:05 a downward ramp occurs, which is only caught by the “Min” strategy. Still, there are times where none of the nowcasts predict a ramp and consequently all break the limit (e.g. 13:40).

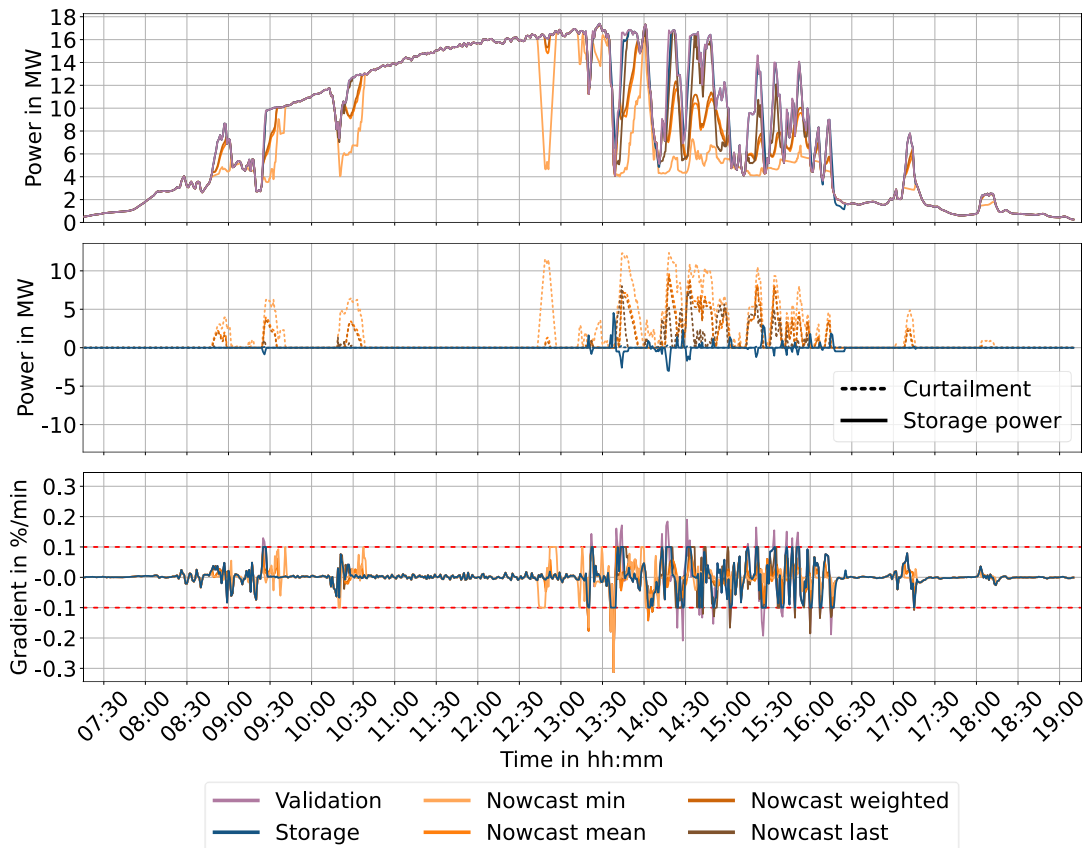


Figure 5.4: Performance charts of storage and nowcasting configurations for one exemplary day (2020/09/02). From top to bottom: graph of power output, graph of curtailment and storage power, graph of gradient. The horizontal dashed red lines in the bottom graph indicate the ramp rate limit of 10 %/min.

The storage strategy, shown in blue, operates very differently. It only steps in when a ramp would otherwise break the limit and does so with 100 % success. 13:40 shows an example where a down ramp is followed by an up ramp. First, the storage is discharged (positive storage power in the middle graph) to prevent the downward ramp rate violation. Then, during the following up ramp, it is charged (negative storage power). The effective curtailment in the output power is visible in the top graph in places where the blue line deviates from the violet validation curve. During charging

a very small uptick in the dashed blue curtailment line is visible. This is caused by the losses that occur when applying the efficiency factor to the charging power. When a down ramp happened and no immediate up ramp follows to restore the SOC, the storage is charged nevertheless in order to prevent the possibility of the storage being empty and unable to smooth ramps. This happens at a reduced constant power to not create any ramps. An example of this process is observed at 16:20.

The 100 % success rate of the storage strategy hinges on the sufficient power and capacity of the storage. In this case it has been designed to be able to mitigate all ramps.

The comparison shows the trade-off that exists in the nowcasting strategies between curtailment and ramp rate compliance. Either a strategy curtails a lot and consequently is able to smooth many ramps (“Min”), or it curtails much more carefully and misses a lot of ramps in the process (“Last”). This fact also plays a major role in the later economic analysis. Additionally, the potential of the storage strategy to mitigate all ramps is demonstrated.

Figure 5.5 shows the performance graphs for the hybrid strategies. The power curves in the top graph look very similar to the nowcasting curves, which is caused by the shared algorithms for administering curtailment. Contrary to the nowcasting strategies however, the curtailment (especially in the first half of the day) is not actually curtailed but rather stored in the battery. The storage powers in the middle graph demonstrate this behaviour. Since the storage is not discharged during normal operation, it reaches maximum capacity at some point and can't be charged any further. Depending on the amount of curtailment proposed by the different nowcasting algorithms, this point is reached sooner or later. For the “Min” strategy this happens around 12:45 when the bright green line suddenly switches from charging the storage to curtailing. The previously described efficiency losses which occur during charging and are counted towards the curtailment are more clearly visible due to the generally higher storage powers. Looking at the gradients, all strategies comply with the ramp rate limit. This is caused by the large storage stepping in whenever the nowcasting fails to predict a ramp. The amount of times this is necessary however, varies depending on the strategy. Those time stamps, where the violet validation curve exceeds the gradient limit and a green line hits the dashed red line and continues horizontally, occur much more often for the dark “Last” line than for the brighter ones, indicating the frequent necessity for the storage to step in.

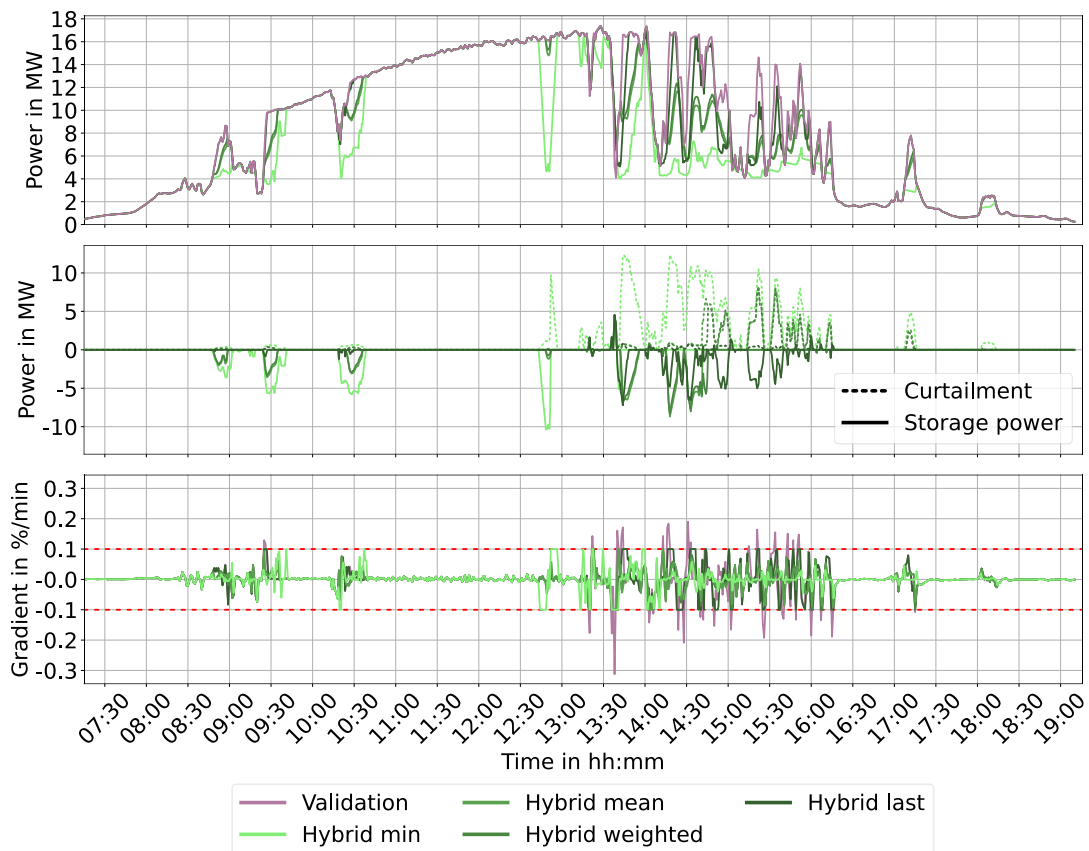


Figure 5.5: Performance charts of hybrid configurations for one exemplary day (2020/09/02). From top to bottom: graph of power output, graph of curtailment and storage power, graph of gradient. The horizontal dashed red lines in the bottom graph indicate the ramp rate limit of 10 %/min.

These charts demonstrate the ability of the nowcasting algorithms to work together with a storage system and store the curtailed energy as far as possible. Furthermore, they show how the storage is utilized to mitigate ramps that are missed by the nowcasting and thus improves the overall performance.

5.2.2. Full year performance analysis

The exemplary day provides great insight into the intricacies that distinguish the different strategies from each other and lead to different results. However, a more cumulative analysis is necessary to make a statement about the overall performance across the complete year. For this, Table 5.2 lists the added-up results of all days combined. Direct output refers to the energy that is fed directly from the PV system to the grid, without taking a detour through the storage. The curtailment column lists the sum of the combined curtailment and storages losses over the entire year. Storage output contains both, the energy that is discharged during the day and thus part of the

fed-in system power, as well as the potential night time discharge from SOC recovery. Combining the three energy readings of any strategy equals the direct output of the validation case. The ramps of each day are counted and added up and lastly the worst and average gradients are determined.

Table 5.2: Performance comparison of all major strategies for the complete year

Strategy	Energy [MWh]			Ramps [#, %/min, %/min]		
	Direct output	Curtailment	Storage output	Missed	Max. gradient	Mean gradient
Validation	34,702.83	0	0	8754	-56.97	-15.44
Base case	34,608.88	93.96	0	4108	-56.97	-15.13
Ideal nowcast	34,525.9	176.93	0	0	-	-
Storage	34,603.28	9.96	89.6	0	-	-
Nowcast min	31,921.56	2781.27	0	725	-36.21	-14.59
Nowcast mean	33,734.76	968.07	0	1899	-48.53	-14.45
Nowcast weighted	33,834.07	868.76	0	2014	-46.66	-14.39
Nowcast last	34,445.55	257.29	0	3359	-46.61	-14.65
Hybrid min	31,925.34	1828.24	949.25	0	-	-
Hybrid mean	33,739.27	337.65	625.92	0	-	-
Hybrid weighted	33,838.33	275.15	589.35	0	-	-
Hybrid last	34,455.8	29.81	217.23	0	-	-

Referring to the top section of the table, the overall performance of the base case and ideal nowcast strategy can be compared. Of the original 8754 ramps present in the validation power data, around half are up ramps that are mitigated by the base case strategy. The necessary curtailment is just around 94 MWh, reducing the direct output only marginally. As a beneficial side effect, the curtailment of up ramps also mitigates down ramps that directly follow these up ramps and don't occur if the power is not allowed to increase as quickly. This explains the overall reduction in ramp count by more than half. Roughly doubling the previous curtailment, the ideal nowcast is able to reduce the number of ramps to zero.

In the bottom section the rest of the strategies are listed and important result are color-coded with red being considered a poor and green a good performance. As to be expected, the storage strategy features the lowest curtailment. It is solely caused by losses during charging, since it equals exactly 1/9 of the storage output (10 % of the original charging energy) and thus correlates with the efficiency factor of 90 %. Supporting the previous observations, the nowcasting strategies show different aggressivities, leading to varying amounts of curtailment and numbers of missed

ramps. “Min” is found to be the strategy with the highest curtailment and lowest number of missed ramps, followed by “Mean” and “Weighted”, which are fairly similar in their results. “Last” curtails the least and consequently missed the most ramps. Comparing the remaining ramp gradients, the best performing nowcasting strategy “Min” is able to reduce the maximum ramp from $-57\%/min$ to around $-36\%/min$. “Last”, “Weighted” and “Mean” don’t achieve as much of a reduction and are between -46 and $-49\%/min$. The mean gradient experiences a slight reduction of around 1% and does not significantly vary between strategies.

Both, the amount of curtailment and the missed ramps are reduced by the introduction of storage systems in the hybrid strategies. The remaining curtailment is partly caused by the storage losses, mostly though the result of the storage being full and not able to store the curtailed energy anymore. Because the battery power and size for the hybrid configurations are the same as for the storage configuration, the number of missed ramps is also reduced to zero. A reduction and optimization of the storage power and correlated capacity is performed in section 5.3.4 and part of the economic analysis. Here, the results are generated with the 2C storage designed in section 3.1.2. A C-rate of 1 would further reduce the curtailment but would also lead to higher costs due to the doubling of capacity. However, these aspects are not relevant at this stage. The general working principle of the hybrid strategies is again demonstrated by the virtually identical direct outputs of the corresponding nowcast and hybrid configurations. As already mentioned, the sums of the three listed energies for each configuration are all equal to the validation power. Since this is the case, it is also derived that no additional energy besides the validation is used and thus the storage never finishes below its target SOC and never needs night time recharge (only discharge).

5.3. Economic results

Following the analysis of the technological potential, the next section includes the economic calculations. Based on the obtained results, the economic potential of the various strategies is investigated and compared.

5.3.1. Base case and ideal nowcast

First, the theoretical potential of nowcasting is analysed by comparing the ideal nowcast against the base case. Since both are unsuitable or unrealistic solutions, they are benchmarked without the introduction of penalties. This leads to a fairer comparison and offers the opportunity to validate the LCOE of the base case with real-world findings.

Table 5.3 lists the relevant economic results of the validation, base case and ideal nowcast. Imbalance costs and profit are yearly values and assumed invariant over the entire lifetime. Since the validation case never curtails, the imbalance costs are zero and the profit consists only of the day-ahead earnings. The base case has to pay some imbalance costs for the curtailment of up ramps, reducing the yearly profit in the process. Similar to the amount of curtailment shown in Table 5.2, the ideal nowcast roughly doubles the imbalance costs. For both, base case and ideal nowcast, the influence of the reduced profit on the LCOE and the NPV is marginal. Ideal nowcast is performing slightly worse, which can be explained by the increased curtailment as well as the investment and operating costs of the nowcasting system.

Table 5.3: Economic comparison of base case and ideal nowcast

	Validation	Base case	Ideal nowcast
Imbalance costs [EUR/a]	0	5445	10,263
Profit [EUR/a]	2,039,156	2,033,712	2,028,894
LCOE [ct/kWh]	3.42	3.42	3.44
Net present value [EUR]	13,198,966	13,114,833	12,990,259

Validation basically represents a typical utility scale PV installation, operated in a grid code without ramp limitations. Because of this, the calculated LCOE can be compared with current real-world data. Lazard’s Levelized Cost of Energy Analysis [93] provides a range of 24 - 96 USD/MWh \approx 2.16 - 8.64 EURct/MWh for 2023. The calculated 3.42 ct/kWh are at the lower end of this spectrum, but well within the bounds. The below average LCOE can be explained by fairly ideal conditions in southern Spain and lower costs compared to the United States.

All three strategies exhibit very high net present values and thus are considered profitable investments. However, without any incentive for ramp rate mitigation, the validation case provides the highest NPV and is therefore the preferred option under these circumstances. Still, base case and the theoretical ideal nowcast offer the potential to mitigate half or even all of the ramps with only very minor losses.

5.3.2. Penalties

Since real nowcasts will never achieve the ideal performance and thus net present values are expected to be much lower, incentives in the form of penalties are introduced.

As described in section 3.3.2 the penalty factor p for both, the fee and the tax penalty scheme, ultimately determines the economically bearable number of ramps and the level of worthwhile investment to comply with the ramp rate limit. The goal of any potential penalty scheme is to make ramp rate non-compliance economically

unattractive. Therefore, the penalty factors for this analysis are calculated by setting the net present value of the base case to zero. In doing so, it is no longer profitable to run a PV plant without any means of mitigating down ramps. In the following, the factors are calculated for both penalty schemes.

The formula for the net present value in Equation (4.3) can be simplified if equal cashflows exist for all periods [90]. This is true for the base case, as no reinvestment costs for a storage or nowcasting system accrue. Equation (5.4) shows the simplified formula. The investment costs of the base case contain only the PV system's costs I_{PV} . Likewise, the operating costs of the PV system C_{PV} are the sole contributors to the overall operating costs. Rewriting the profit R_{bc} according to Equation (5.5), the desired penalty costs $C_{p,bc}$ appear. The profit without penalties $R_{bc,np}$ is listed in Table 5.3. Note the correction for the six missing days in the simulation (also refer to section 4.3.3).

$$NPV_{bc} = -I_{PV} + (R_{bc} - C_{PV}) * \frac{(1+i)^{L_{PV}} - 1}{(1+i)^{L_{PV}} * i} \quad (5.4)$$

$$R_{bc} = R_{bc,np} * \frac{365 \text{ d}}{359 \text{ d}} - C_{p,bc} * \frac{365 \text{ d}}{359 \text{ d}} \quad (5.5)$$

Inserting (5.5) into (5.4) and solving for $C_{p,bc}$ yields Equation (5.6).

$$C_{p,bc} = R_{bc,np} - \left(C_{PV} + \frac{NPV_{bc} + I_{PV}}{(1+i)^{L_{PV}} - 1} \right) * \frac{359}{365} \quad (5.6)$$

All necessary values are either known or can be calculated. They are listed in Table 5.4 for reference.

Table 5.4: Necessary values for penalty factor calculation

Parameter	Value	Reference
$R_{bc,np}$	2,033,712 EUR/a	Table 5.3
NPV_{bc}	0 EUR	
I_{PV}	$CAPEX_{PV} * P_{PV,max} = 14,291,098 \text{ EUR}$	Table 3.1
C_{PV}	$OPEX_{PV} * P_{PV,max} = 264,533 \text{ EUR/a}$	Table 3.1
L_{PV}	30 a	Table 3.1
i	0.051	Section 4.3.3

Inserting them yields the desired yearly penalty costs of the base case that are necessary to achieve the net present value of zero (Eq. (5.7)).

$$C_{p,bc} = 848,703.95 \frac{\text{EUR}}{\text{a}} \quad (5.7)$$

Based on these penalty costs, the penalty factors of the two schemes are calculated. Rearranging Equation (3.17), Equation (5.8) gives the factor for the fee penalty scheme of around 4669 EUR/MWh. The ramp rate violation energy of the base case $E_{NC,bc}$ is 181.79 MWh (see Table C.2 in the appendix).

$$p_{fee} = \frac{C_{p,bc}}{E_{NC,bc}} \approx 4668.59 \frac{\text{EUR}}{\text{MWh}} \quad (5.8)$$

Combining and rearranging Equations (3.18), (3.19) and (3.20), a formula for the tax penalty factor is derived. Since the tax factor TF changes every week, depending on the non-compliance, the profit and the ratio of non-compliant time steps need to be evaluated in weekly intervals and added up afterwards. Equation (5.9) shows the final result of this process.

$$p_{tax} = \frac{C_{p,bc}}{\sum_{w=1}^{53} R_{bc,np,w} * \frac{n_{NC,w}}{n_{t,w}}} \approx 49.9 \quad (5.9)$$

Before starting with the detailed economic analysis, the two different penalty schemes, fee and tax, are compared against each other in order to find similarities and differences. A total of 19 unique configurations are presented during the course of this analysis, 17 of which implement penalties. A complete list of the configurations and the corresponding results can be found in appendix C. These 17 configurations are processed with both, the fee and tax penalty scheme and the results are compared. Table 5.5 shows the summarized findings. Even though both penalty factors were calculated by setting the NPV of the base case to zero, the tax penalty scheme ended up imposing slightly smaller penalty costs when applied onto all configurations. These differences however, don't have a large impact. The NPV ranking consistency of 100 % means that in both schemes all configurations are ranked the same when sorted by net present value. Absolute and relative NPV deviations between the two schemes are also low. The absolute Bias is negative, meaning the NPVs are generally higher in the tax penalty scheme (due to lower average costs). Relative to the net present value of each configuration however, the Bias is slightly positive. This is due to small absolute deviations leading to higher relative deviations for configurations where the NPV is relatively low.

Table 5.5: Comparison between fee and tax penalty schemes

		Fee	Tax
Average costs [EUR/MWh]		4668.59	4655.16
NPV ranking consistency [%]		100	
Absolute NPV deviation [EUR]	Max.	132,939	
	Bias	-13,539	
	MAE	87,791	
Relative NPV deviation [%]	Max.	5.53	
	Bias	0.39	
	MAE	1.56	

Overall, with a relative MAE of less than 1.6 %, the differences between the schemes are considered negligible and therefore only the fee penalty scheme is chosen for the further analysis.

5.3.3. Nowcast and storage

After implementation of the penalties, the non-ideal nowcasting strategies are analysed and benchmarked against the designed storages and the base case. Figure 5.6 shows the yearly penalties, imbalance costs and resulting profit as well as the net present value and the LCOE with and without penalties for all seven strategies. Looking at the penalties, the four nowcasting strategies exhibit major reductions in the yearly costs compared to the base case. Correlating with the number of ramps shown in Table 5.2, “Min” achieves the lowest penalty costs of the four strategies. Due to their successful mitigation of all ramps, both storage configurations, the 1C and the 2C, pay zero penalties. Except during active ramp prevention and recharging to the target SOC, the storages also don’t cause any further imbalances, which refers to deviations from the day-ahead trades, and therefore achieve very low imbalance costs. The imbalance costs of the nowcasting strategies show a reverse arrangement to the penalties. They correlate with the curtailment (see Table 5.2) and thus “Min” experiences the highest and “Last” the lowest costs. The fact that the base case does not feature lower imbalance costs than the storage configurations is caused by the potential compensation of negative with positive imbalance and vice versa by the storages during the 15-minute settlement periods (section 4.3.2).

Low imbalance costs and no penalty payments lead to the highest profits for the storage configurations. The nowcasting strategies generate lower profits, proportionally to the sum of penalties and imbalance costs. Since they outperform the base case, the imbalance costs caused by curtailment are clearly overcompensated by the savings in penalty payments. This also leads to “Min” achieving the highest profits of the four strategies.

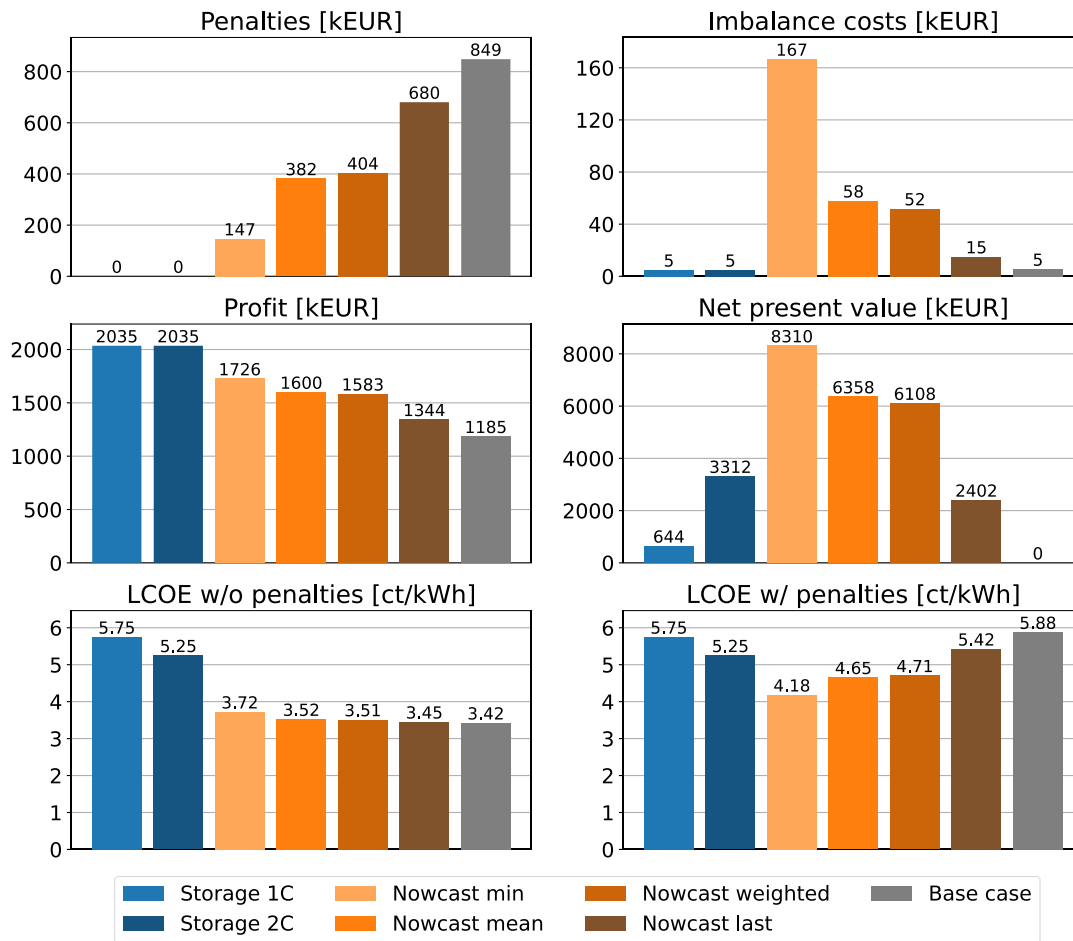


Figure 5.6: Economic comparison of nowcasting and designed storage configurations

Until now the results were directly correlated to the physical performance of the configurations. This changes with the net present value. Here the investment and operating costs are also taken into consideration. This especially shows in the poor performance of the storages. Despite generating the highest yearly profits by far, their NPVs are at the lower end of the spectrum, with the 1C storage only barely above zero. The nowcasts capitalize on their low system costs, resulting in higher net present values. Of all seven strategies “Nowcast min” is the superior option with the highest NPV of more than 8 million EUR.

Because of the high system costs, the storage configurations also have the highest LCOEs. The obtained 5.25 and 5.75 ct/kWh are within the range for utility scale PV systems with storage determined by Lazard [93]. The LCOEs without penalties are subject to the costs of the system and the amount of energy sold. Even though the system costs are the same, “Nowcast min” possesses the highest LCOE of all nowcasting strategies as it feeds in less energy due to higher curtailment. The LCOEs with penalties include the penalty payments and show the influence they have on

energy costs. Higher penalties obviously lead to larger deviations from the non-penalty LCOE with “Nowcast last” exhibiting a delta of almost 2 ct/kWh. As expected, the LCOE with penalties mirrors the ranking order of the net present values among the strategies, with “Nowcast min” emerging as the top performer with an LCOE of 4.18 ct/kWh.

The increase in energy costs caused by the investigated ramp mitigating regulation, represented by penalties, is obtained by comparing the LCOE with penalties of “Nowcast min” against the LCOE without penalties of the base case. The result is an increase of 0.76 ct/kWh.

This analysis shows the great potential of nowcasting in a regulatory environment that features ramp penalties. Not only does it provide a comfortably positive net present value and therefore a valid business case, it also, depending on the strategy applied, outperforms the designed storage configurations. However, the mitigation of ramps comes at a cost. Comparing the NPV of “Nowcast min” against the NPV of the base case scenario without regulations (see Table 5.3), a total reduction of almost 5 million EUR is observed. This is supported by the aforementioned increase in LCOE.

As seen in Figure 5.6 and also observed in the sensitivity analysis in section 5.4, a C-rate of $CR = 2$ is always superior to $CR = 1$. This is due to the large oversizing of the storage (see section 3.1.2), which is less extreme for $CR = 2$. Thus, only the higher rated configurations are analysed in further detail.

5.3.4. Optimization and hybrid

So far, the hybrid strategies have been omitted from the economic analysis. That’s because it is not economically viable to combine a nowcasting system with the same large designed storage that is also used for the separate storage configuration. In such a combination the nowcasting would not add any value to the system. The hybrid strategies are only relevant if their potential to reduce the storage needs compared to the standalone storage configuration is considered. Furthermore, when full ramp rate compliance is not considered essential anymore, refining the optimal economic solution becomes attainable for the standalone storage configuration as well. Achieving this enhancement involves decreasing the power and size of the battery.

Consequently, a sensitivity analysis with varying maximum storage powers is performed. Whereby a C-rate of $CR = \frac{P_{bat}}{C_{bat}} = 2$ is maintained and the storage capacity set accordingly. All four hybrid configurations as well as the storage configuration are optimized for a maximum net present value. The results of the sensitivity analysis are shown in Figure 5.7.

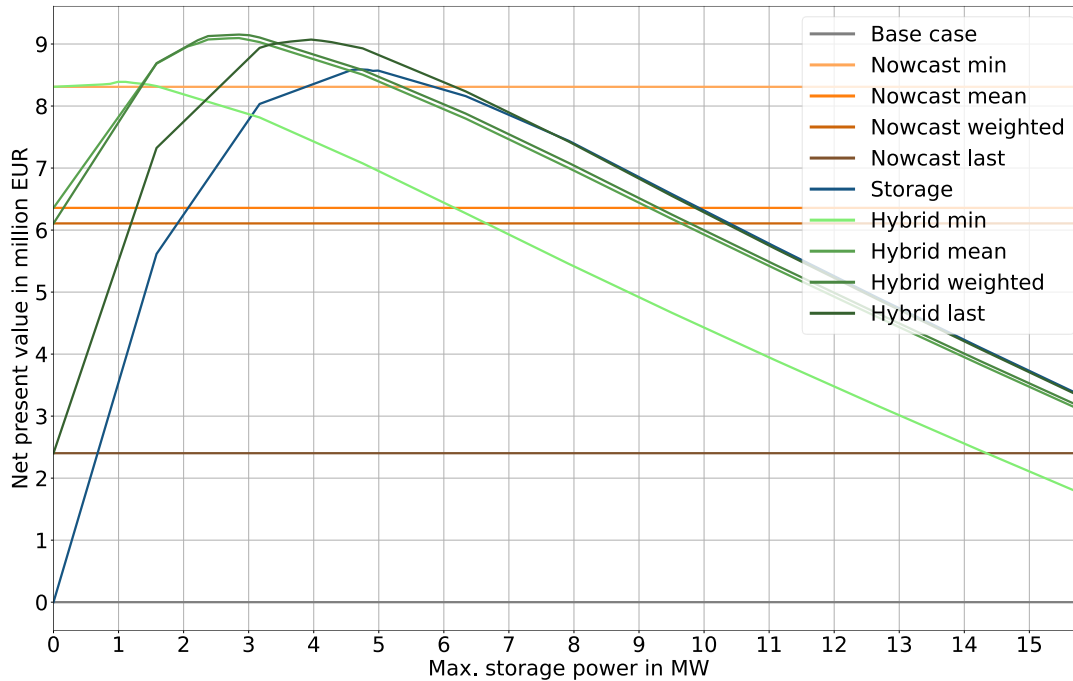


Figure 5.7: Sensitivity analysis of the net present value to different maximum storage powers

All curves that correspond to a configuration with storage show a clear maximum. Their shape demonstrates the two competing influences on the net present value. Left of the optimum, the number of missed ramps increases and penalty costs become too high. On the right, the storage gets too large and the increasing system costs overpower the benefits.

For reference, the net present values of the non-storage strategies are also plotted. At a storage power of 0 the hybrid configurations are indistinguishable from their nowcasting counterparts and consequently line up with them at this point. The storage strategy lines up with the base case. At the right end of the graph the NPVs for the originally designed storage power (section 3.1.2) can be read. By comparing with the maximum values, it becomes evident how economically inadequate such a high storage power is.

Two general observations are made from this analysis. Firstly, the lower the number of missed ramps and consequently the higher the NPV of a nowcasting strategy is, the smaller the benefits from adding a storage are. “Hybrid min” for example is only barely able to surpass the “Nowcast min” line. Secondly, hybrid configurations that use less aggressive nowcasting strategies need bigger storages to reach their optimum. By extension, the standalone storage configuration needs the largest battery.

Using the results of the sensitivity analysis, the ideal storage power for each of the configurations is chosen and listed in Table 5.6. Note that the accuracy of these

optimums is limited by the resolution of the sensitivity analysis, which was 1 % of the designed power ($\sim 160,000$ W) directly around the maximums.

Table 5.6: Optimized maximum storage powers

Configuration	Max. storage power [W]
Storage	4,751,928
Hybrid min	989,985
Hybrid mean	2,851,157
Hybrid weighted	2,851,157
Hybrid last	3,959,940

Before comparing the optimized storage and hybrid configurations, the results of the strategy with the highest net present value, “Hybrid weighted” are presented in greater detail. A complete collection of inputs and results for all 19 investigated configurations is attached in appendix C.

Table 5.7 lists the utilized inputs for the “Hybrid weighted” configuration. The previously determined maximum storage power from Table 5.6 is used and the corresponding specific storage costs $CAPEX_{bat}$ and $OPEX_{bat}$ are obtained according to section 3.1.2. Multiplying the specific investment costs with the maximum power gives the total investment costs for the storage system (Eq. (5.10)).

$$I_{bat} = CAPEX_{bat} * P_{bat,max} = 1,751,238 \text{ EUR} \quad (5.10)$$

The yearly operating costs are derived according to Equation (5.11).

$$C_{bat} = OPEX_{bat} * P_{bat,max} = 35,025 \frac{\text{EUR}}{\text{a}} \quad (5.11)$$

Investment and operating costs of the nowcasting system are listed in Table 5.7 and the costs of the PV system have been calculated in Table 5.4.

Table 5.7: Detailed inputs of the hybrid weighted configuration

Description	Variable name	Unit	Value
Configuration	<i>config</i>	-	hybrid
Nowcast strategy	<i>nc_strat</i>	-	weighted
Ramp rate limit	<i>r_{lim}</i>	[%/min]	10
Max. storage power	<i>P_{bat,max}</i>	[W]	2,851,157
C-rate	<i>CR</i>	-	2
Target idle SOC	<i>soc_aim</i>	-	0.5
SOC equalizing factor	<i>dump_limit</i>	<i>r_{lim}</i>	0.5
Penalty scheme	<i>p_scheme</i>	-	fee
Penalty factor	<i>p_{fee}</i>	[EUR/MWh]	4668.59
Discount rate	<i>i</i>	-	0.051
PV investment costs	<i>CAPEX_{PV}</i>	[EUR/kWp]	676.38
PV operating costs	<i>OPEX_{PV}</i>	[EUR/kWp/a]	12.52
Storage investment costs	<i>CAPEX_{bat}</i>	[EUR/kW]	614.22
Storage operating costs	<i>OPEX_{bat}</i>	[EUR/kW/a]	12.28
Nowcasting investment costs	<i>CAPEX_{NC}</i>	[EUR]	25,000
Nowcasting operating costs	<i>OPEX_{NC}</i>	[EUR/a]	1430

These inputs are utilized and the results in Table 5.8 are generated.

Adding the direct output and the storage output at daytime yields the yearly system output during daytime of almost 33.9 GWh.

Combining this with the storage output at night and subtracting the result from the validation energy gives the curtailment and storage losses of 681 MWh during one year of operation.

Of the total 463,322 simulated time steps, 264 remain with gradients above the ramp rate limit and entail a ramp rate violation energy of almost 12 MWh. Inserting into Equation (3.17) yields the penalty costs of 55,708 EUR per year. These, together with C_{imb} and R_{SOC} reduce the day-ahead earnings and give the final yearly profit of 1.944 million EUR. LCOE and NPV are calculated according to Equations (4.2) and (4.3) with all costs, benefits and energies remaining constant for all 30 years of operation. The only exception is year 16 where the storage and nowcasting systems reach their end of life and need reinvestment of 30 % of the original costs (calculated in Equation (5.10) and listed in Table 5.7 respectively) (also refer to section 4.3.3).

Table 5.8: Detailed results of the hybrid weighted configuration

Description	Variable name	Unit	Value
Validation energy	E_{val}	[MWh]	34,702.83
Direct output	E_{dir}	[MWh]	33,837.46
Storage output at day	$E_{bat,day}$	[MWh]	24.48
System output at day	$E_{sys,day}$	[MWh]	33,861.94
Storage output at night	$E_{bat,night}$	[MWh]	159.88
Total storage output	$E_{bat,tot}$	[MWh]	184.36
Curtailment and storage losses	E_{curt}	[MWh]	681.01
Number of missed ramps	n_{NC}	-	264
Number of time steps	n_t	-	463,322
Max. ramp gradient	r_{max}	[%/min]	-33.16
Mean ramp gradient	r_{mean}	[%/min]	-15.67
Ramp rate violation energy	E_{NC}	[MWh]	11.93
Day-ahead benefits	B_{da}	[EUR]	2,039,156
Imbalance costs	C_{imb}	[EUR]	50,592
Equalize SOC net cash flow	R_{SOC}	[EUR]	10,810
Profit before penalties	R_{np}	[EUR]	1,999,374
Penalty costs	C_p	[EUR]	55,708
Profit	R	[EUR]	1,943,666
LCOE without penalties	$LCOE_{np}$	[ct/kWh]	3.97
LCOE with penalties	$LCOE_p$	[ct/kWh]	4.14
Net present value	NPV	[EUR]	9,152,650

For the analysis and comparison of the technological performance of “Hybrid weighted” and the other strategies, their performance parameters, previously shown in Table 5.2 need to be updated in order to reflect the changes in storage powers and capacities. The updated results of the optimized configurations are listed in Table 5.9. “Nowcast min” is also shown for comparison purposes.

Except for some minor rounding errors, the direct output of all strategies stays the same as in Table 5.2. However, the less powerful and smaller storages have an effect on the storage outputs, which are lower than before. Subsequently, curtailment values are higher.

Table 5.9: Performance comparison of strategies with optimized storages for the complete year

Strategy	Direct output	Energy [MWh]		Ramps [#, %/min, %/min]		
		Curtailement	Storage output	Missed	Max. gradient	Mean gradient
Storage	34,604.96	11.73	86.14	246	-34.48	-14.73
Nowcast min	31,921.56	2781.27	0	725	-36.21	-14.59
Hybrid min	31,923.24	2701.77	77.82	370	-34.02	-15.04
Hybrid mean	33,738.25	776.87	187.72	253	-35.04	-15.77
Hybrid weighted	33,837.46	681.01	184.36	264	-33.16	-15.67
Hybrid last	34,454.73	95.47	152.63	227	-28.19	-14.79

Looking at the ramps, all strategies now feature a low three-digit number of missed ramps, with “Hybrid last” performing best in terms of number of ramps and maximum gradient. This is likely the cause of having the largest storage of all hybrid configurations and the ability to predict some ramps compared to the standalone storage setup.

While all optimized configurations manage to outperform “Nowcast min” when it comes to missed ramps and maximum gradient, they actually are worse when comparing the mean gradient. One explanation for this circumstance is the fact that the storage power is only sufficient for smoothing smaller ramps and fails to prevent larger ones, thus shifting the average. This is supported by the observation that “Hybrid last”, having the largest storage, achieves the highest reduction in maximum gradient compared to “Nowcast last”. The other strategies with smaller storages achieve much smaller changes, with “Hybrid min”, having by far the smallest storage, only improving by 2 percentage points over its purely nowcasting counterpart.

Next, the final economic analysis is performed. Just like the previous performance comparison, the five optimized configurations are benchmarked against the best standalone nowcasting configuration “Nowcast min”. The results are displayed in Figure 5.8. Compared to Figure 5.6, adding the storage systems enabled the hybrid configurations to drastically reduce the number of missed ramps and subsequently the penalty costs. All of them outperform the most conservative nowcasting strategy with penalties between 46 and 76 kEUR/a compared to 147 kEUR/a. Imbalance costs remain more or less identical to the nowcasting counterparts, since the total imbalance volumes, i.e. the delta between validation energy and actual direct output, are not significantly influenced by the introduction of storages.

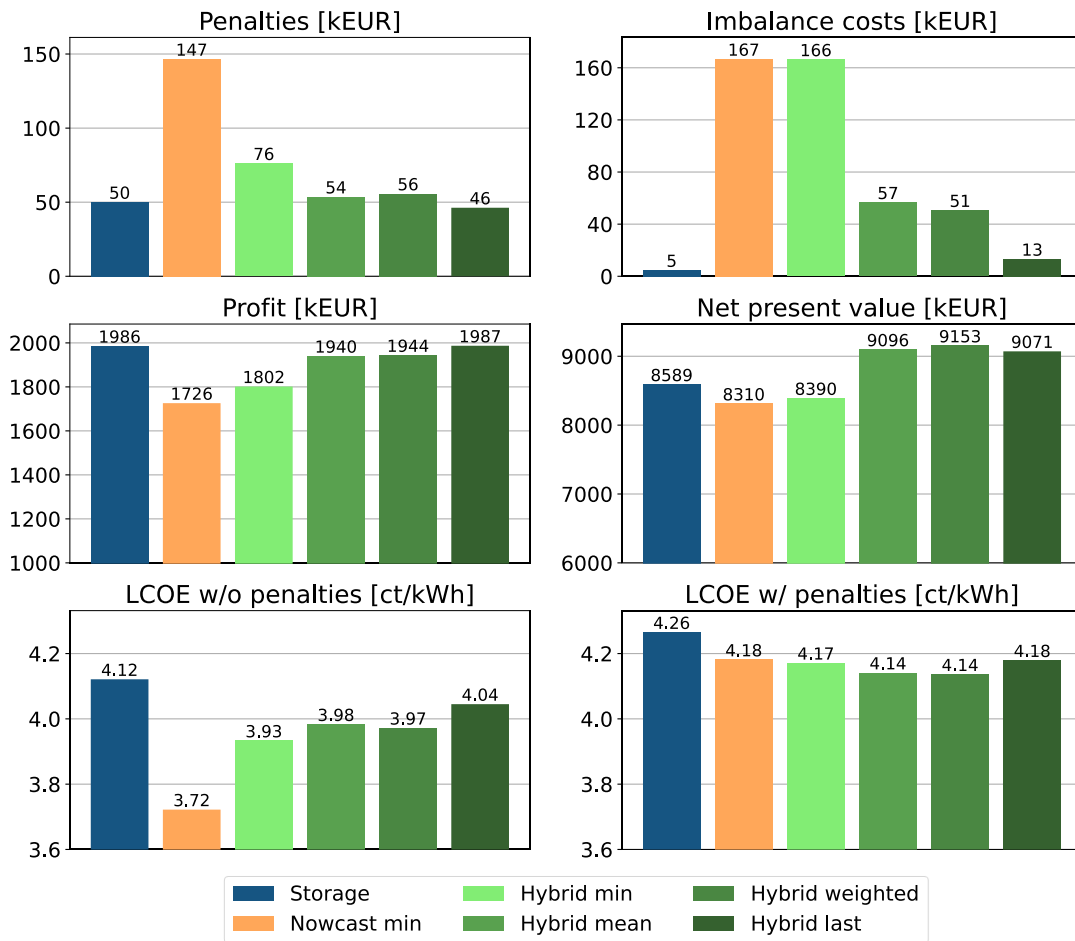


Figure 5.8: Economic comparison of optimized storage and hybrid configurations

Looking at the yearly profit, “Storage” and “Hybrid last” share the top spot with virtually equal values. All hybrid configurations manage to improve compared to the respective standalone nowcasting strategies and even surpass “Nowcast min”. The storage setup is the only one that experiences a slight reduction in profit compared to Figure 5.6 due to the zero penalty costs in the original configuration.

Analysing the net present value, it is apparent that all optimized configurations outperform “Nowcast min”. Although, the overall differences are much smaller than in the previous comparison. “Hybrid weighted” is identified as the most profitable investment, very closely followed by “Mean” and “Last”. “Hybrid min” offers only a small improvement over “Nowcast min” and can’t compete with other hybrid strategies. Contrary to the previous comparison, the optimized storage configuration is now superior to standalone nowcasting, though not as profitable as most of the hybrid strategies.

While “Nowcast min” has the highest LCOE without penalties of all the standalone nowcasting strategies, all hybrid configurations surpass “Nowcast min” due to the

addition of storages. The hybrid setup with the largest storage, “Hybrid last”, now possesses the highest LCOE of the four configurations. This increase overpowers the expected reduction due to reduced curtailment and consequently more sold energy compared to the nowcasting counterparts. “Storage” manages to reduce its LCOE significantly due to the smaller battery, however still features the biggest storage of the compared configurations and thus has the highest LCOE.

Adding the penalties to the calculation changes the picture. While “Storage” is still the most expensive option, it is now followed by “Nowcast min” and “Hybrid last”. “Hybrid weighted”, the strategy with the highest NPV also features the lowest LCOE of 4.14 ct/kWh and thus is considered the overall economically best option for the given circumstances. The total minimum increase in energy costs compared to the base case without any penalty scheme now is 0.72 ct/kWh.

Besides the finding of the best strategy, the analysis also shows that when no storage is present, high curtailment is bearable and conservative nowcasting strategies perform best. Apart from that, less conservative and more aggressive strategies are superior in combination with a storage. Another important observation is the fact that nowcasting alone cannot compete with an optimally designed storage. However, due to the relatively small differences in NPV and the lower investment costs, the nowcasting configuration might be more accessible and still be a viable business case.

Ultimately, each strategy has its own strength. “Nowcast min” entails low investment costs, “Storage” features low curtailment, “Hybrid last” has a low number of missed ramps and “Hybrid weighted” provides the highest net present value.

5.4. Sensitivity analysis

The analyses in postprocessing are based on many input parameters with some of them being subject to uncertainties. In order to analyse their influence on the results a sensitivity analysis is performed. A total of eight critical parameters are determined and used as variables. The output metric for comparison is chosen to be the net present value. Figure 5.9 shows the results for seven of the eight relevant parameters. The influence of the maximum storage power has already been presented in Figure 5.7.

Each subplot features the variable being adjusted on the x-axis, either as absolute values or as relative factors. A black dashed line pinpoints the original value used in the previous analyses. In most subplots the NPV is shown for four different strategies: the overall best hybrid setup “Hybrid weighted”, the highest performing nowcasting “Nowcast min”, the optimized storage and the base case. Each representing the best option achievable with the approach used. Some plots omit the base case, due to it being out of scope or not of interest for a certain parameter.

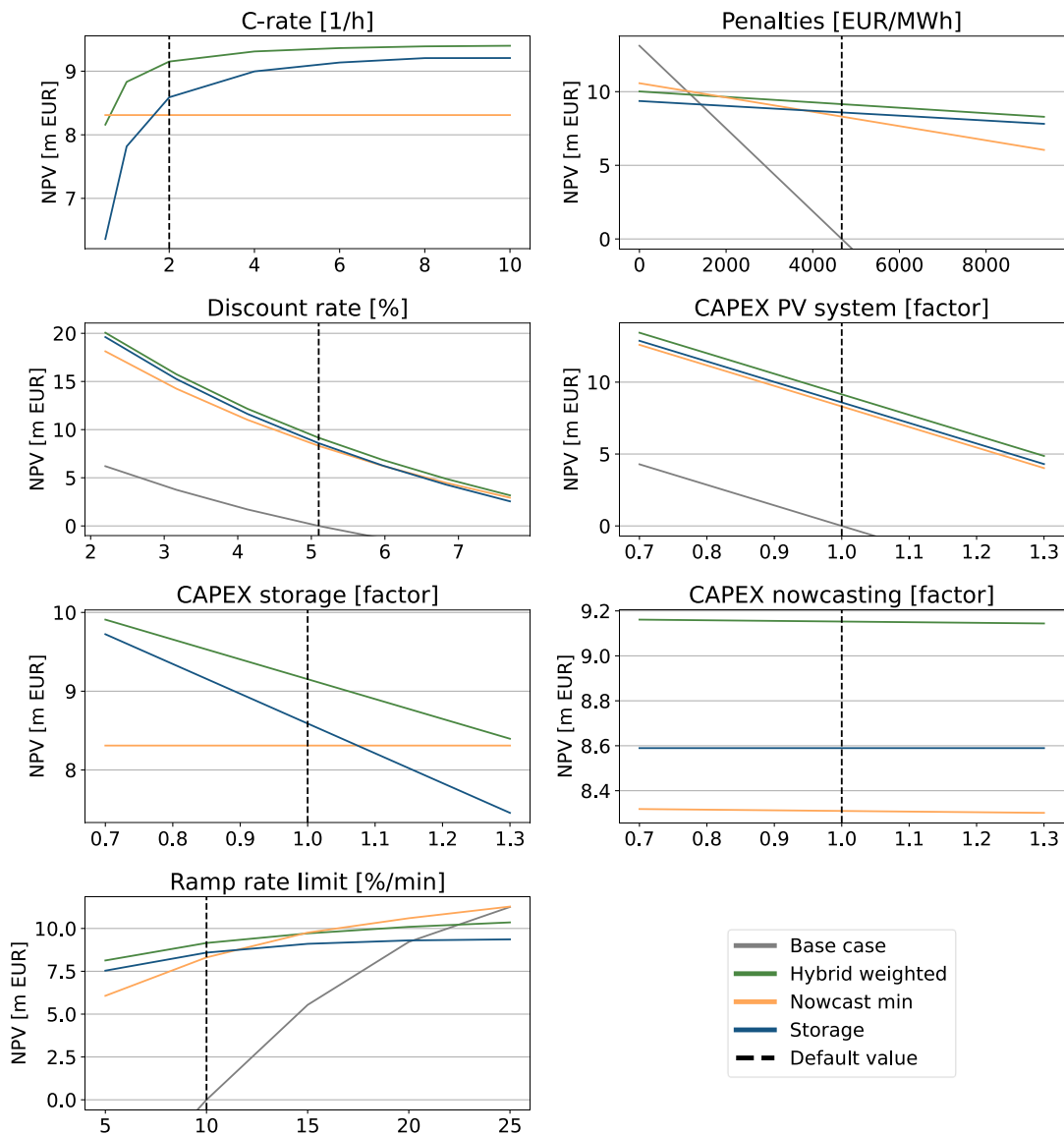


Figure 5.9: Sensitivity analysis of the net present value to seven different parameters. The coloured lines represent the optimized configurations. The vertical line shows the default value of the respective parameter.

Starting with variation of the C-rate, the results clearly show the benefit of higher C-rates for both battery-containing configurations. Interestingly, the C-rate of 6, determined in section 3.1.2 is not the economic optimum but rather even higher rates are to be preferred. It should be noted however, that especially the cost extrapolation is highly inaccurate at these high C-rates, as they would necessitate different battery technologies and do not represent currently feasible configurations. Further, a

potential optimization regarding the maximum power at different C-rates is not considered.

The penalties are a central assumption in this work and their value has been defined by setting the NPV of the base case to zero. As to be expected, variations in the penalties affect those strategies most, that contain the highest number of missed ramps. This leads to intersections of the (linear) NPV curves, where other strategies become more or less viable. The lower the penalties, the less its worth to invest in ramp rate mitigation measures and “Nowcast min” and “Base case” become more profitable. Higher penalties lead to superiority of the storage-containing configurations. The exact point where an intersection happens can’t be determined this way, since the changes in optimal storage sizes and strategies are not taken into account.

Discount rate has the strongest influence of all examined parameters on the overall net present values. The boundaries for the sensitivity analysis are set to the lowest value found in literature (2.2 % for Germany in [91]) and the most recent estimation by Lazard (7.7 % for the USA in [93]). On the one hand, when taking the rate for Germany, the net present values of all strategies more than double compared to Spain. However, it should be noted that the low discount rates for Germany are from a period before 2022 with historically low interest rates, which are no longer attained. On the other hand, when taking the recent estimations for the USA, the NPVs are less than half of the default values. This shows, that very high discount rates, as currently the trend, could present a serious challenge for the investigated configurations but also for any investment in general. While no big differences between the configurations are observed, the effect seems to be slightly larger on configurations with higher investment costs.

The influence of the investment costs on the net present values is examined next. Split into separate analyses for the costs of each component and varying them by $\pm 30\%$, three main conclusions are drawn. As expected, the PV system costs equally influence all configurations, as they share the same PV plant. Higher costs obviously reduce the NPV and vice versa. The CAPEX of the storage system only affects the NPVs of the setups that implement a storage, particularly those with larger batteries. If the costs rise too much, the storage-containing configurations become unattractive and standalone nowcasting presents the better business case. Again, the exact costs at which this happens cannot be determined from this graph, since the storage sizes would first get reduced in order to adapt to the higher costs. The third observation concerns the nowcasting system. Its costs are found to be so low, that changes are barely noticeable in the final NPV. The almost negligible influence of the nowcasting costs justifies the relatively uncertain estimation of them in the first place (section 3.1.3).

Besides the shown CAPEX, the OPEX of a system also influences the net present value. Although not plotted, the observed effects of CAPEX variations are transferable to OPEX variations with the NPV curves demonstrating the same behaviour. For all three systems the absolute influence of the OPEX is smaller than the CAPEX's.

Lastly, different ramp rate limits are investigated. As to be expected, stricter limits favour more consistent solutions, namely "Hybrid weighted" and "Storage". More lax limits lead to less ramps in general and thus investment into mitigation becomes less sensible. At some point, even the base case outperforms all other configurations.

As with all previous sensitivity analyses, the purpose is just to show tendencies and no absolute results. The latter would require constant recalculation of the proper penalty factor, optimization of the storage power and new selection of the best performing strategy for every adjustment made and consequently would exceed the scope of this thesis.

Overall, the analysis demonstrates the reliability of the implemented postprocessing tool, as no unexpected results from parameter variations are observed. Furthermore, the influences of uncertain assumptions such as the penalties, discount rate and nowcasting costs are examined and used to better gauge the final results.

6. Conclusion

This thesis analysed the techno-economic potential of nowcasting to reduce the impact of irradiance ramps on PV power production. For this, a virtual power plant was placed at the location of CIEMAT's PSA in southern Spain. Ambient measurements of several meteorological stations across the site were obtained for a time frame of one year and processed into a validation dataset containing the actual current irradiance, temperature, pressure and wind speed conditions at every time step. Additionally, probabilistic nowcasts from all-sky imagers with a resolution of 30 seconds and 10-minute lead times were generated and provided short-term predictions of the irradiance for every time step. Both, the validation and irradiance nowcasts were used as inputs for a detailed model of the PV system. The PV model has been developed in a previous work [16] but was adapted and improved to suit the use case. In it, the irradiance maps provided by validation and nowcasts were used to calculate the power output of each PV module, considering the local irradiance. The individual powers were combined and transformed, resulting in the AC power output of the entire plant. Since validation and nowcasts were used as inputs, the model generated a validation power output as well as a set of power nowcasts for the immediate future for every time step of the year.

The validation power output of the standalone PV plant was found to contain a lot of high gradients. Gradients higher than 10 % of the maximum power output per minute were defined as critical ramps. This definition corresponds to the most widely used definition in various grid codes around the world (see section 2.4).

Several algorithms were developed to control the fed-in power output and reduce the number of ramps by making use of either nowcasts with preemptive curtailment, a storage system or a combination of both. All algorithms proved successful, with a large storage being the most reliable way of mitigating all ramps while featuring no noteworthy curtailment. The best performing nowcasting algorithm managed to reduce the number of down ramps from 4108 to 725 just by detecting high gradients in the power predictions and curtailing preemptively. Down ramps are especially critical since unlike up ramps they cannot be mitigated through reactive curtailment but rather need preemptive curtailment or a battery to step in.

For the economic analysis, the power control algorithms were appended by a marketing strategy and placed in a regulatory framework which imposed penalties

dependant on the remaining ramps and the energy necessary to mitigate them. The marketing strategy calculated the yearly profits by trading electricity at the markets and paying penalties. Together with investment and operating costs, the profits were used to calculate the net present value and levelized cost of energy of any specific configuration.

Nowcasting algorithms were then combined with storages to form hybrid configurations, the powers and capacities of which were optimized for yielding the maximum net present value, thus meeting the sweet spot between high system costs and high penalty payments.

Table 6.1 presents an overview of the results of the techno-economic analysis conducted under the regulated ramp rate environment. “Hybrid weighted”, a nowcasting strategy where the lead times are weighted according to their accuracy combined with a medium-sized storage, exhibited the highest NPV of all configurations and thus is considered the optimal strategy under the given penalty regulations. 264 down ramps were missed by this setup, a reduction of more than 93 % from the original 4108 down ramps. Comparison of the NPV with the standalone storage solution clearly shows the benefit of nowcasting. The hybrid solution achieved a net present value almost 600,000 EUR higher, while implementing a 40 % smaller storage, thus saving resources and investment costs. Even though standalone nowcasting cannot quite compete with a storage solution, it is much more accessible regarding costs and resource needs and especially the conservative “Min” strategy still provides a very profitable investment.

Table 6.1: Overview of selected final results: The analysis includes the base case without any measures against down ramps, along with the outcomes of the best standalone nowcasting and storage strategies, as well as the best hybrid strategy. All presented results reflect the outcome under a regulated ramp rate environment.

Strategy	Storage size [kW]	Missed ramps -	NPV [kEUR]	LCOE [ct/kWh]
Base case	0	4108	0	5.88
Nowcast min	0	725	8310	4.18
Storage	4752	246	8589	4.26
Hybrid weighted	2851	264	9153	4.14

However, the ability to mitigate ramps comes at a cost. The “Hybrid weighted” configuration loses around 4,000,000 EUR net present value compared to a PV plant in a completely unregulated ramp rate environment. This large deviation is the sum of higher investment costs and lower profit due to curtailment and penalties. Similar

observations were made when comparing the LCOEs, with the costs being 0.72 ct/kWh higher than in an unregulated environment.

Ultimately, nowcasting and especially hybrid configurations not only show great technological potential for smoothing the output power and reducing volatility, but also provide the economically best solution under the investigated circumstances.

In order to keep investments in renewable energy attractive, different or additional regulations might need to be considered. System operators also need to decide on the exact objective that a potential ramp mitigating regulation should achieve. This objective could be having no ramps at all, limiting the ramps to a manageable number or, as implemented in this work, reducing the overall amount of needed balancing energy or balancing power, all while keeping the curtailment as low as possible. Regulations would need to incentivise investment into the solutions that achieve this goal the best and ideally not reduce the net present value in the process.

Considering future developments, the potential of nowcasting is expected to increase even further. The development of more accurate nowcasts and better algorithms for power control will decrease the number of missed ramps and especially the faulty curtailment significantly and thus improve the overall performance. Better nowcasts also reduce the storage needs in the hybrid configurations. Decreases in storage costs not only influence the standalone storage setups but additionally make hybrid solutions more attractive.

While this thesis provided a qualitative analysis of nowcasting and its use cases, further research is necessary in order to obtain reliable quantitative economic results. Key points that need further research are:

- More detailed simulations of the battery system with cycles, aging and refurbishment
- implementation of smarter control strategies such as introduced in [71] and [13]
- utilization of storages for additional services
- optimization of the nowcast data processing
- investigation of sites with more challenging weather conditions
- utilization of higher resolved validation data or actual power data
- implementation of a more detailed and realistic marketing strategy
- determination of a use-case-specific discount rate
- consideration of settling times for power set points as well as investigation of new battery technologies with higher C-rates
- other potential regulations regarding ramp rate limitation [94] and penalisation

7. Bibliography

- [1] European Commission, *European Green Deal: EU agrees stronger legislation to accelerate the rollout of renewable energy*. 2023.
- [2] Edenhofer, O., et al., *Renewable energy sources and climate change mitigation: special report of the Intergovernmental Panel on Climate Change*. Choice Reviews Online, 2012. 49(11): p. 49-6309-49-6309 DOI: <https://doi.org/10.5860/choice.49-6309>.
- [3] Mohandes, B., et al., *A Review of Power System Flexibility With High Penetration of Renewables*. IEEE Transactions on Power Systems, 2019. 34(4): p. 3140-3155 DOI: <https://doi.org/10.1109/tpwrs.2019.2897727>.
- [4] Huber, M., D. Dimkova, and T. Hamacher, *Integration of wind and solar power in Europe: Assessment of flexibility requirements*. Energy, 2014. 69: p. 236-246 DOI: <https://doi.org/10.1016/j.energy.2014.02.109>.
- [5] Holttinen, H., *Impact of hourly wind power variations on the system operation in the Nordic countries*. Wind Energy, 2005. 8(2): p. 197-218 DOI: <https://doi.org/10.1002/we.143>.
- [6] Makarov, Y.V., et al., *Operational Impacts of Wind Generation on California Power Systems*. IEEE Transactions on Power Systems, 2009. 24(2): p. 1039-1050 DOI: <https://doi.org/10.1109/tpwrs.2009.2016364>.
- [7] Gevorgian, V. and S. Booth, *Review of PREPA Technical Requirements for Interconnecting Wind and Solar Generation*. 2013, Office of Scientific and Technical Information (OSTI).
- [8] Zheng, Q., et al. *Overview of grid codes for photovoltaic integration*. 2017. IEEE.
- [9] Haghighat, M., M. Niroomand, and H.D. Tafti, *An Adaptive Power Ramp Rate Control Method for Photovoltaic Systems*. Ieee Journal of Photovoltaics, 2022. 12(2): p. 557-564 DOI: <https://doi.org/10.1109/Jphotov.2021.3133408>.
- [10] Ramasamy, V., et al., *U.S. Solar Photovoltaic System and Energy Storage Cost Benchmarks, With Minimum Sustainable Price Analysis: Q1 2022*. 2022, National Renewable Energy Laboratory (NREL).
- [11] van Haaren, R., *Utility Scale Photovoltaic Plant Variability Studies and Energy Storage Optimization for Ramp Rate Control*. 2014.
- [12] Cirés, E., et al., *The potential of forecasting in reducing the LCOE in PV plants under ramp-rate restrictions*. Energy, 2019. 188 DOI: <https://doi.org/10.1016/j.energy.2019.116053>.
- [13] Patarroyo-Montenegro, J.F., et al., *Comparative and Cost Analysis of a Novel Predictive Power Ramp Rate Control Method: A Case Study in a PV Power Plant in Puerto Rico*. Applied Sciences-Basel, 2021. 11(13): p. 5766 DOI: <https://doi.org/10.3390/app11135766>.

- [14] Saleh, M., et al., *Battery-Less Short-Term Smoothing of Photovoltaic Generation Using Sky Camera*. Ieee Transactions on Industrial Informatics, 2018. 14(2): p. 403-414 DOI: <https://doi.org/10.1109/Tii.2017.2767038>.
- [15] Sengupta, M., et al., *Best Practices Handbook for the Collection and Use of Solar Resource Data for Solar Energy Applications: Third Edition*. 2021, National Renewable Energy Laboratory.
- [16] Schaible, J., *Application of nowcasting to reduce the impact of irradiance ramps on PV power plants*. 2022.
- [17] International Energy Agency, *Renewables 2022 Analysis and forecast to 2027*. 2022.
- [18] Einstein, A., *Über einen die Erzeugung und Verwandlung des Lichtes betreffenden heuristischen Gesichtspunkt*. Annalen der Physik, 1905. 322(6): p. 132-148 DOI: <https://doi.org/10.1002/andp.19053220607>.
- [19] Quaschnig, V., *Regenerative Energiesysteme Technologie - Berechnung - Simulation ; mit 319 farbigen Bildern, 119 Tabellen und einer DVD*. 2015, Hanser: München.
- [20] National Renewable Energy Laboratory (NREL). *Best Research-Cell Efficiency Chart*. 2023 [Accessed: 2023/06/02]; Available from: <https://www.nrel.gov/pv/cell-efficiency.html>.
- [21] Crawley, G.M., *Solar energy*. World Scientific series in current energy issues Volume 2. 2016, New Jersey: World Scientific.
- [22] Pinto, T., Z. Vale, and S. Widergren, *Local electricity markets*. 2021, London: Elsevier.
- [23] Weber, C., D. Möst, and W. Fichtner, *Economics of Power Systems Fundamentals for Sustainable Energy*. 1st 2022 ed. Springer Texts in Business and Economics. 2022, Cham: Springer International Publishing.
- [24] ENTSO-E. *ENTSO-E Transparency Platform*. 2023 [Accessed: 2023/06/05]; Available from: <https://transparency.entsoe.eu/dashboard/show>.
- [25] Lopes, F. and H. Coelho, *Electricity Markets with Increasing Levels of Renewable Generation: Structure, Operation, Agent-based Simulation, and Emerging Designs*. Studies in Systems, Decision and Control 144. 2018, Cham: Springer International Publishing.
- [26] OMIE. *Details of the intraday market's operation*. Available from: https://www.omie.es/sites/default/files/inline-files/intraday_and_continuous_markets.pdf.
- [27] OMIE. *Intraday price*. 2023 [Accessed: 2023/06/05]; Available from: <https://www.omie.es/en/market-results/daily/intradaily-market/intradaily-market-price?>
- [28] Rodilla, P. and C. Batlle, *Empirics of Intraday and Real-time Markets in Europe: Spain*. 2015, DIW - Deutsches Institut für Wirtschaftsforschung.
- [29] Red Eléctrica. *Markets and Prices*. 2023 [Accessed: 2023/06/05]; Available from: <https://www.esios.ree.es/en/market-and-prices?date=05-06-2023#>.

- [30] International Renewable Energy Agency (IRENA), *Grid Codes for Renewable Powered Systems* 2022.
- [31] Australian Energy Market Commission (AEMC), *National Electricity Rules Version 194*. 2023.
- [32] Australian Energy Market Commission (AEMC), *National Electricity Amendment (Generator Technical Performance Standards) Rule 2018*. 2018.
- [33] Western Power, *Technical Rules*. 2016.
- [34] Horizon Power, *Horizon Power Technical Rules Standard Number: HPC-9DJ-01-0001-2012*. 2022.
- [35] Horizon Power, *Low Voltage EG Connection Technical Requirements Standard Number: HPC-9DJ-13-0002-2019*. 2021.
- [36] Australian Energy Market Operator (AEMO), *Regulation FCAS Contribution Factor Procedure*. 2023.
- [37] Atherton, J., R. Sharma, and J. Salgado, *Techno-economic analysis of energy storage systems for application in wind farms*. Energy, 2017. 135: p. 540-552 DOI: <https://doi.org/10.1016/j.energy.2017.06.151>.
- [38] Standardization Administration of the People's Republic of China, *GB/T 19964-2012 Technical requirements for connecting photovoltaic power station to power system*. 2012.
- [39] Energinet.dk, *Technical regulation 3.2.2 for PV power plants above 11 kW*. 2016.
- [40] Khan, B., et al., *A Review of Grid Code Requirements for the Integration of Renewable Energy Sources in Ethiopia*. Energies, 2022. 15(14): p. 5197 DOI: <https://doi.org/10.3390/en15145197>.
- [41] VDE, *Technische Anschlussregel Mittelspannung (VDE-AR-N 4110)* 2018.
- [42] *Erneuerbare-Energien-Gesetz* 2023; Available from: https://www.gesetze-im-internet.de/eeg_2014/__9.html.
- [43] Central Electricity Authority, *Central Electricity Authority Notification No.12/X/STD(CONN)/GM/CEA/2018*. 2019.
- [44] EirGrid Group, *EirGrid Grid Code Version 11*. 2022.
- [45] Khan, R. and Y. Go, *Assessment of Malaysia's Large-Scale Solar Projects: Power System Analysis for Solar PV Grid Integration*. Glob Chall, 2020. 4(2): p. 1900060 DOI: <https://doi.org/10.1002/gch2.201900060>.
- [46] Suruhanjaya Tenaga Energy Commission, *Guidelines On Large Scale Solar Photovoltaic Plant For Connection To Electricity Networks [Electricity Supply Act (Amendment) 2015 (Act A1501)]*. 2018.
- [47] Puerto Rico Electric Power Authority (PREPA), *Minimum Technical Requirements for Interconnection of Photovoltaic (PV) Facilities*.
- [48] Makibar, A., L. Narvarte, and E. Lorenzo, *On the relation between battery size and PV power ramp rate limitation*. Solar Energy, 2017. 142: p. 182-193 DOI: <https://doi.org/10.1016/j.solener.2016.11.039>.

- [49] Villena-Ruiz, R., et al., *Requirements for New Grid Codes: A Review in Spain & Portugal*, in *20th International Conference on Renewable Energies and Power Quality (ICREPQ'22)*. 2022.
- [50] Martínez-Lavín, M., et al., *Evaluation of the latest Spanish grid code requirements from a PV power plant perspective*. *Energy Reports*, 2022. 8: p. 8589-8604 DOI: <https://doi.org/10.1016/j.egy.2022.06.078>.
- [51] Nouri, B., et al., *A Hybrid Solar Irradiance Nowcasting Approach: Combining All Sky Imager Systems and Persistence Irradiance Models for Increased Accuracy*. *Solar RRL*, 2021. 6(5): p. 2100442 DOI: <https://doi.org/10.1002/solr.202100442>.
- [52] Fabel, Y., et al., *All-sky imager based irradiance nowcasts: combining a physical and a deep learning model*. 2022, ISES.
- [53] Nouri, B., et al., *Probabilistic solar nowcasting based on all-sky imagers*. *Solar Energy*, 2023. 253: p. 285-307 DOI: <https://doi.org/10.1016/j.solener.2023.01.060>.
- [54] Schroedter-Homscheidt, M., et al., *Classifying ground-measured 1 minute temporal variability within hourly intervals for direct normal irradiances*. *Meteorologische Zeitschrift*, 2018. 27(2): p. 161-179.
- [55] Sterner, M. and I. Stadler, *Energiespeicher – Bedarf, Technologien, Integration*. 2 ed. 2017, Berlin, Heidelberg: Springer Berlin Heidelberg.
- [56] International Renewable Energy Agency (IRENA), *Innovation landscape brief: Utility-scale batteries*. 2019 DOI: <https://doi.org/https://doi.org/10.1007/978-92-9260-139-3>.
- [57] Marcos, J., et al., *Storage requirements for PV power ramp-rate control*. *Solar Energy*, 2014. 99: p. 28-35 DOI: <https://doi.org/10.1016/j.solener.2013.10.037>.
- [58] Figgenger, J., et al., *The development of battery storage systems in Germany: A market review (status 2023)*. arXiv pre-print server, 2023 DOI: <https://doi.org/https://doi.org/10.1007/978-92-9260-139-3>.
- [59] International Renewable Energy Agency (IRENA), *Electricity Storage Valuation Framework: Assessing system value and ensuring project viability*. 2020.
- [60] Commission, E., et al., *Study on energy storage*. 2023: Publications Office of the European Union.
- [61] Loevenich, M. and L. Kaborn, *Dokumentation Internes Tool zur Ertragsberechnung in Python*. 2020.
- [62] F. Holmgren, W., C. W. Hansen, and M. A. Mikofski, *pvlb python: a python package for modeling solar energy systems*. *Journal of Open Source Software*, 2018. 3(29): p. 884 DOI: <https://doi.org/10.21105/joss.00884>.
- [63] California Energy Commission. *PV Module List - Full Data*. [Accessed: 2023/05/12]; Available from: <https://www.energy.ca.gov/media/2367>.
- [64] Kratochvil, J., W. Boyson, and D. King, *Photovoltaic array performance model*. 2004 DOI: <https://doi.org/10.2172/919131>.

- [65] Dobos, A., *PVWatts Version 5 Manual*. 2014, Office of Scientific and Technical Information (OSTI).
- [66] California Energy Commission. *Solar Equipment List - CA Energy Commission*. [Accessed: 2023/05/12]; Available from: <https://solarequipment.energy.ca.gov/Home/InverterSolarList>.
- [67] Kost, C., et al., *Stromgestehungskosten Erneuerbarer Energien*. 2021, Fraunhofer-Institut für Solare Energiesysteme ISE.
- [68] International Renewable Energy Agency (IRENA), *Renewable Power Generation Costs in 2021*. 2022.
- [69] National Renewable Energy Laboratory (NREL). *Annual Technology Baseline: Utility-Scale PV*. 2022 [Accessed: 2023/06/08]; Available from: https://atb.nrel.gov/electricity/2022/utility-scale_pv.
- [70] Solargis s.r.o., *Ground albedo data - Tabernas, Spain - Technical Report*. 2020.
- [71] de la Parra, I., et al., *Control strategies to use the minimum energy storage requirement for PV power ramp-rate control*. *Solar Energy*, 2015. 111: p. 332-343 DOI: <https://doi.org/10.1016/j.solener.2014.10.038>.
- [72] Keil, P., et al., *Calendar Aging of Lithium-Ion Batteries*. *Journal of The Electrochemical Society*, 2016. 163(9): p. A1872-A1880 DOI: <https://doi.org/10.1149/2.0411609jes>.
- [73] Motapon, S.N., et al., *A Generic Cycle Life Model for Lithium-Ion Batteries Based on Fatigue Theory and Equivalent Cycle Counting*. *IEEE Open Journal of the Industrial Electronics Society*, 2020. 1: p. 207-217 DOI: <https://doi.org/10.1109/ojies.2020.3015396>.
- [74] Lai, C.S., et al., *Levelized cost of electricity for photovoltaic/biogas power plant hybrid system with electrical energy storage degradation costs*. *Energy Conversion and Management*, 2017. 153: p. 34-47 DOI: <https://doi.org/10.1016/j.enconman.2017.09.076>.
- [75] National Renewable Energy Laboratory (NREL). *Annual Technology Baseline: Utility-Scale Battery Storage*. 2022; Available from: https://atb.nrel.gov/electricity/2022/utility-scale_battery_storage.
- [76] National Renewable Energy Laboratory (NREL). *Annual Technology Baseline: Commercial Battery Storage*. 2022; Available from: https://atb.nrel.gov/electricity/2022/commercial_battery_storage.
- [77] Augustine, C. and N. Blair, *Energy Storage Futures Study: Storage Technology Modeling Input Data Report*. 2021, National Renewable Energy Laboratory (NREL).
- [78] Eurostat. *Labour cost levels by NACE Rev. 2 activity*. 2022; Available from: https://ec.europa.eu/eurostat/databrowser/view/lc_lci_lev/default/table?lang=en.

- [79] Wen, H.R., et al., *Deep Learning Based Multistep Solar Forecasting for PV Ramp-Rate Control Using Sky Images*. Ieee Transactions on Industrial Informatics, 2021. 17(2): p. 1397-1406 DOI: <https://doi.org/10.1109/Tii.2020.2987916>.
- [80] Sangwongwanich, A., Y. Yang, and F. Blaabjerg. *A cost-effective power ramp-rate control strategy for single-phase two-stage grid-connected photovoltaic systems*. 2016. IEEE.
- [81] Riquelme-Dominguez, J.M., F.D. Garcia-Lopez, and S. Martinez, *Power Ramp-Rate Control via power regulation for storageless grid-connected photovoltaic systems*. International Journal of Electrical Power & Energy Systems, 2022. 138 DOI: <https://doi.org/10.1016/j.ijepes.2021.107848>.
- [82] Martins, J., et al., *Comparative Study of Ramp-Rate Control Algorithms for PV with Energy Storage Systems*. Energies, 2019. 12(7): p. 1342 DOI: <https://doi.org/10.3390/en12071342>.
- [83] Demain, C., M. Journée, and C. Bertrand, *Evaluation of different models to estimate the global solar radiation on inclined surfaces*. Renewable Energy, 2013. 50: p. 710-721 DOI: <https://doi.org/10.1016/j.renene.2012.07.031>.
- [84] Yang, D., *Solar radiation on inclined surfaces: Corrections and benchmarks*. Solar Energy, 2016. 136: p. 288-302 DOI: <https://doi.org/10.1016/j.solener.2016.06.062>.
- [85] Blum, N.B., *Nowcasting of Solar Irradiance and Photovoltaic Production Using a Network of All-Sky Imagers*. 2022.
- [86] Red Eléctrica, *Red Eléctrica will adapt the operation schedule of the peninsular electricity system into 15-minute periods*. 2022.
- [87] OMIE. *Electricity market*. 2023 [Accessed: 2023/06/05]; Available from: <https://www.omie.es/en/mercado-de-electricidad>.
- [88] Bueno-Lorenzo, M., M.Á. Moreno, and J. Usaola, *Analysis of the imbalance price scheme in the Spanish electricity market: A wind power test case*. Energy Policy, 2013. 62: p. 1010-1019 DOI: <https://doi.org/10.1016/j.enpol.2013.08.039>.
- [89] Konstantin, P., *Praxisbuch Energiewirtschaft Energieumwandlung, -transport und -beschaffung im liberalisierten Markt*. 2013, Springer Berlin Heidelberg: Berlin, Heidelberg.
- [90] Gerke, W. and M. Bank, *Finanzierung*, in *Grundlagen für Investitions- und Finanzierungsentscheidungen im Unternehmen*. 2016, W. Kohlhammer Verlag.
- [91] International Renewable Energy Agency (IRENA), *The cost of financing for renewable power*. 2023.
- [92] Samu, R., et al., *Applications for solar irradiance nowcasting in the control of microgrids: A review*. Renewable and Sustainable Energy Reviews, 2021. 147 DOI: <https://doi.org/10.1016/j.rser.2021.111187>.
- [93] Lazard and R. Berger, *Lazard's Levelized Cost of Energy Analysis—Version 16.0*. 2023.

-
- [94] Gevorgian, V., M. Baggu, and D. Ton, *Interconnection Requirements for Renewable Generation and Energy Storage in Island Systems: Puerto Rico Example: Preprint*. 2019.

Appendices

A. PV module parameters

Table A.1: PV module parameters [63, 64]

Parameter	Value	Parameter	Value
Name	REC_Solar_REC265PE	Adjust	2.915298
Technology	Multi-c-Si	gamma_r	-0.4464
Bifacial	0	BIPV	N
STC	265.122	Version	SAM 2018.11.11 r2
PTC	241.3	Date	1/3/2019
A_c	1.587	A0	0.9219
Length	1.641	A1	0.0709
Width	0.967	A2	-0.0143
N_s	60	A3	0.0012
I_sc_ref	9.08	A4	-3e-05
V_oc_ref	38.1	B0	1
I_mp_ref	8.58	B1	-0.0024
V_mp_ref	30.9	B2	0.0003103
alpha_sc	0.003532	B3	-1.246e-05
beta_oc	-0.130378	B4	2.11e-07
T_NOCT	44.6	B5	-1.36e-09
a_ref	1.562064	DTC	3
I_L_ref	9.082499	A	-3.56
I_o_ref	2.310707e-10	B	-0.075
R_s	0.301464	FD	1
R_sh_ref	1095.698364		

B. Factors for nowcast weighting

Table B.1: Factors for nowcast weighting

Lead time	Factor [%]	Lead time	Factor [%]	Lead time	Factor [%]
LT0	6.733	LT3.5	5.117	LT7	3.959
LT0.5	6.656	LT4	4.908	LT7.5	3.829
LT1	6.578	LT4.5	4.736	LT8	3.698
LT1.5	6.214	LT5	4.564	LT8.5	3.56
LT2	5.851	LT5.5	4.412	LT9	3.421
LT2.5	5.589	LT6	4.259	LT9.5	3.3
LT3	5.327	LT6.5	4.109	LT10	3.179

C. Detailed inputs and results

Table C.1: Detailed inputs of all presented configurations. np = no penalties, p = penalties, wtd = weighted, des = designed, opt = optimized. For explanation of the variables refer to Table 5.7 and Table 5.8

Variable	Unit	Validation		Base case np		Base case p		Ideal nowcast		Storage 1C des		Storage 2C des		Storage 2C opt		Nowcast min		Nowcast mean	
		validation	fec	base_case np	fec	base_case p	fec	fec	ideal_nowcast	storage	fec	storage	fec	storage	fec	storage	nowcast min	nowcast mean	
<i>config</i>	-	validation	fec	base_case np	fec	base_case p	fec	ideal_nowcast	storage	fec	storage	fec	storage	fec	storage	nowcast min	nowcast mean		
<i>nc_strat</i>	-	-	-	-	-	-	-	-	-	-	-	-	-	-	-	min	mean		
<i>r_{tim}</i>	[%/min]	10	10	10	10	10	10	10	10	10	10	10	10	10	10	10	10		
<i>P_{bat,max}</i>	[W]	0	0	0	0	0	0	0	15,839,760	15,839,760	15,839,760	15,839,760	4,751,928	4,751,928	0	0	0		
<i>CR</i>	-	-	-	-	-	-	-	-	1	2	2	2	2	2	-	-	-		
<i>soc_aim</i>	-	-	-	-	-	-	-	-	0.5	0.5	0.5	0.5	0.5	0.5	-	-	-		
<i>dump_limit</i>	<i>r_{tim}</i>	-	-	-	-	-	-	-	0.5	0.5	0.5	0.5	0.5	0.5	-	-	-		
<i>p_scheme</i>	-	fec	fec	fec	fec	fec	fec	fec	fec	fec	fec	fec	fec	fec	fec	fec	fec		
<i>p_{fee}</i>	[EUR/MWh]	0	0	4668.59	4668.59	4668.59	4668.59	4668.59	4668.59	4668.59	4668.59	4668.59	4668.59	4668.59	4668.59	4668.59	4668.59		
<i>i</i>	-	0.051	0.051	0.051	0.051	0.051	0.051	0.051	0.051	0.051	0.051	0.051	0.051	0.051	0.051	0.051	0.051		
<i>CAPEX_{pv}</i>	[EUR/kWp]	676.38	676.38	676.38	676.38	676.38	676.38	676.38	676.38	676.38	676.38	676.38	676.38	676.38	676.38	676.38	676.38		
<i>OPEX_{pv}</i>	[EUR/kWp/a]	12.52	12.52	12.52	12.52	12.52	12.52	12.52	12.52	12.52	12.52	12.52	12.52	12.52	12.52	12.52	12.52		
<i>CAPEX_{bat}</i>	[EUR/kW]	-	-	-	-	-	-	-	548.1	431.05	552.72	552.72	552.72	552.72	-	-	-		
<i>OPEX_{bat}</i>	[EUR/kW/a]	-	-	-	-	-	-	-	10.96	8.62	11.05	11.05	11.05	11.05	-	-	-		
<i>CAPEX_{NC}</i>	[EUR]	-	-	-	-	-	-	25,000	-	-	-	-	-	-	25,000	25,000	25,000		
<i>OPEX_{NC}</i>	[EUR/a]	-	-	-	-	-	-	1430	-	-	-	-	-	-	1430	1430	1430		

Table C.2: Detailed results of all presented configurations. np = no penalties, p = penalties, wtd = weighted, des = designed, opt = optimized. For explanation of the variables refer to Table 5.7 and Table 5.8

Variable	Unit	Validation	Base case np	Base case p	Ideal nowcast	Storage 1C des	Storage 2C des	Storage 2C opt	Nowcast min	Nowcast mean
E_{bat}	[MWh]	34,702.83	34,702.83	34,702.83	34,702.83	34,702.83	34,702.83	34,702.83	34,702.83	34,702.83
E_{dir}	[MWh]	34,702.83	34,608.88	34,608.88	34,525.9	34,603.28	34,603.28	34,604.96	31,921.56	33,734.76
$E_{bat,day}$	[MWh]	0	0	0	0	76.41	76.41	72.16	0	0
$E_{sys,day}$	[MWh]	34,702.83	34,608.88	34,608.88	34,525.9	34,679.68	34,679.68	34,677.12	31,921.56	33,734.76
$E_{bat,night}$	[MWh]	0	0	0	0	13.19	13.19	13.98	0	0
$E_{bat,tot}$	[MWh]	0	0	0	0	89.6	89.6	86.14	0	0
E_{curt}	[MWh]	0	93.96	93.96	176.93	9.96	9.96	11.73	2781.27	968.07
η_{NC}	-	8754	4108	4108	0	0	0	246	725	1899
η_t	-	463,322	463,322	463,322	463,322	463,322	463,322	463,322	463,322	463,322
τ_{max}	[%/min]	-56.97	-56.97	-56.97	-	-	-	-34.48	-36.21	-48.53
τ_{mean}	[%/min]	-15.44	-15.13	-15.13	-	-	-	-14.73	-14.59	-14.45
E_{NC}	[MWh]	392.78	181.79	181.79	0	0	0	10.71	31.38	81.74
B_{da}	[EUR]	2,039,156	2,039,156	2,039,156	2,039,156	2,039,156	2,039,156	2,039,156	2,039,156	2,039,156
C_{imb}	[EUR]	0	5445	5445	10,263	4796	4796	4610	166,621	57,847
R_{soc}	[EUR]	0	0	0	0	946	946	962	0	0
R_{np}	[EUR]	2,039,156	2,033,712	2,033,712	2,028,894	2,035,306	2,035,306	2,035,509	1,872,535	1,981,309
C_p	[EUR]	0	0	848,704	0	0	0	50,006	146,521	381,626
R	[EUR]	2,039,156	2,033,712	1,185,008	2,028,894	2,035,306	2,035,306	1,985,502	1,726,014	1,599,683
$LCOE_{np}$	[ct/kWh]	3.42	3.42	3.42	3.44	5.75	5.25	4.12	3.72	3.52
$LCOE_p$	[ct/kWh]	3.42	3.42	5.88	3.44	5.75	5.25	4.27	4.18	4.65
NPV	[EUR]	13,198,966	13,114,833	0	12,990,259	643,519	3,312,103	8,589,477	8,309,925	6,357,763

Variable	Unit	Nowcast weighted	Nowcast last	Hybrid min des	Hybrid min opt	Hybrid mean des	Hybrid mean opt	Hybrid wt des	Hybrid wt opt	Hybrid last des	Hybrid last opt
E_{val}	[MWh]	34,702.83	34,702.83	34,702.83	34,702.83	34,702.83	34,702.83	34,702.83	34,702.83	34,702.83	34,702.83
E_{dir}	[MWh]	33,834.07	34,445.55	31,925.34	31,923.24	33,739.27	33,738.25	33,838.33	33,837.46	34,455.8	34,454.73
$E_{bat,day}$	[MWh]	0	0	9.64	4.51	28.48	23.35	29.75	24.48	50.83	46.74
$E_{sys,day}$	[MWh]	33,834.07	34,445.55	31,934.98	31,927.75	33,767.75	33,761.61	33,868.08	33,861.94	34,506.63	34,501.47
$E_{bat,night}$	[MWh]	0	0	939.61	73.32	597.44	164.36	559.60	159.88	166.4	105.89
$E_{bat,tot}$	[MWh]	0	0	949.25	77.82	625.92	187.72	589.35	184.36	217.22	152.63
E_{curr}	[MWh]	868.76	257.29	1828.24	2701.77	337.64	776.87	275.15	681.01	29.81	95.47
η_{NC}	-	2014	3359	0	370	0	253	0	264	0	227
η_t	-	463,322	463,322	463,322	463,322	463,322	463,322	463,322	463,322	463,322	463,322
η_{max}	[%/min]	-46.66	-46.61	-34.02	-34.02	-35.04	-35.04	-33.16	-33.16	-28.19	-28.19
η_{mean}	[%/min]	-14.39	-14.65	-15.04	-15.04	-15.77	-15.77	-15.67	-15.67	-14.79	-14.79
E_{NC}	[MWh]	86.5	145.76	0	16.31	0	11.48	0	11.93	0	9.91
B_{da}	[EUR]	2,039,156	2,039,156	2,039,156	2,039,156	2,039,156	2,039,156	2,039,156	2,039,156	2,039,156	2,039,156
C_{imb}	[EUR]	51,841	14,968	166,032	166,288	56,500	56,637	50,463	50,592	13,156	13,153
R_{soc}	[EUR]	0	0	63,252	4935	40,478	11,106	37,909	10,810	11,120	7236
R_{np}	[EUR]	1,987,316	2,024,189	1,936,376	1,877,804	2,023,134	1,993,625	2,026,603	1,999,374	2,037,124	2,033,240
C_p	[EUR]	403,822	680,491	0	76,156	0	53,597	0	55,708	0	46,255
R	[EUR]	1,583,494	1,343,698	1,936,376	1,801,647	2,023,134	1,940,027	2,026,603	1,943,666	2,037,124	1,986,985
$LCOE_{np}$	[ct/kWh]	3.51	3.45	5.55	3.93	5.31	3.98	5.3	3.97	5.26	4.05
$LCOE_p$	[ct/kWh]	4.71	5.43	5.55	4.17	5.31	4.14	5.3	4.14	5.26	4.18
NPV	[EUR]	6,107,595	2,402,082	1,733,248	8,389,795	3,073,896	9,096,419	3,127,499	9,152,650	3,290,080	9,071,449